5-2017

Development of a low cost biosensing platform for highly sensitive and specific on-site detection of pathogens and infections

Cheng Cheng
University of Tennessee, Knoxville, ccheng8@vols.utk.edu

To the Graduate Council:

I am submitting herewith a dissertation written by Cheng Cheng entitled "Development of a low cost biosensing platform for highly sensitive and specific on-site detection of pathogens and infections." I have examined the final electronic copy of this dissertation for form and content and recommend that it be accepted in partial fulfillment of the requirements for the degree of Doctor of Philosophy, with a major in Electrical Engineering.

Jayne Wu, Major Professor

We have read this dissertation and recommend its acceptance:

Nicole McFarlane, Gong Gu, Shigetoshi Eda

Accepted for the Council:
Dixie L. Thompson

Vice Provost and Dean of the Graduate School

(Original signatures are on file with official student records.)

Development of a low cost biosensing platform for highly sensitive and specific on-site detection of pathogens and infections

A Dissertation Presented for the

Doctor of Philosophy

Degree

The University of Tennessee, Knoxville

Cheng Cheng

May 2017

DEDICATION

This dissertation is dedicated to my beloved parents, Li Yin and Xiaohua Cheng, whose love and encouragement make it possible for me to finish this work.

This dissertation is also dedicated to my best friends Xinyu Yang and Yanfen Liu for always being there for me throughout the process. Both of you have been my best cheerleaders.

ACKNOWLEDGEMENTS

I would like to express my thanks to those who helped me with various aspects of conducting research and writing this dissertation.

First and foremost, I would like to express my deepest gratitude to my advisor, Dr. Jayne Wu for her continuous guidance and persistent help for this dissertation and all other research during my Ph.D. study at the University of Tennessee at Knoxville.

I am very thankful to Dr. Eda Shigetoshi, Dr. Nicole McFarlane and Dr. Gong Gu for their time and efforts in serving as the members of my dissertation committee.

Moreover, I would like to express my special thanks to Dr. Jiangang Chen and Dr. Anming Hu for being supportive to my works as well as their kind advice in my research. Also, I would like to thank all my friends and visiting scholars in our research group who create a loving and friendly atmosphere for conducting research.

ABSTRACT

A highly sensitive, specific, real time, and field-deployable surveillance tool is critical to the control of pathogens and infections, as well as ecological impact of chemicals exposure. This work investigates the development of a low cost biosensing platform that can be used for viral disease diagnosis and chemical detection. The sensing mechanism is known as AC electrokinetics (ACEK) capacitive sensing. By applying an inhomogeneous AC electric field on sensor electrodes, positive dielectrophoresis is induced to accelerate the travel of analytes. The same applied AC signal also directly measures the capture of target by the probe on sensor surface. The realized sensing platform is not only rapid but also highly sensitive and specific. Built on our initial proof-of-concept of ACEK capacitive sensing, this work studies in details the immobilization of probes on electrode surface, electrode design, the interactions between biomolecules such as nucleic acids and testing buffers, and the effect of dielectrophoresis and accompanying ACEK phenomena. Experimental comparisons are made between sensors with various probe immobilization, different electrode designs, testing buffer and detection protocols. As a result, much higher sensitivity and selectivity have been achieved. We are able to successfully detect virus particles in nasal swab samples, specific antibody in serum and whole genome nuclei acids in serum. To extend the application of this sensing method on other electrode platform, polyimide-based laser printed electrodes are also investigated and successfully demonstrated for small molecule detection. However, this type of sensor exhibits high internal resistance, making it only suitable for chemical or particle detection in highly resistive electrolyte, such as de-ionized water. With procedural and design improvements

discussed in this work, it is expected that ACEK capacitive sensing will become a disruptive technology in on-site biochemical detection.

Keywords: capacitive sensing, ACEK, point of care, virus, protein, nucleic acid.

TABLE OF CONTENTS

CHAPTER 1 INTRODUCTION 1

1.1 History, development and challenges of biosensor 1

1.2 Improvement on capacitive sensing 4

CHAPTER 2 LITERATURE REVIEW 5

2.1 Electrochemical enzymatic biosensors 6

2.2 Labeled affinity biosensor 7

2.3 Label-free affinity biosensors 8

CHAPTER 3 AC ELECTROKINETICS 11

3.1 Dielectrophoresis 11

3.2 AC Electroosmosis 12

3.3 AC electrothermal effect 13

3.4 Capacitive sensing 13

CHAPTER 4 ELECTRODES FOR DIRECT CAPACITIVE BIOSENSING 16

4.1 Various interdigitated electrodes 16

4.1.1 Surface acoustic wave (SAW) resonators 16

4.1.2 Copper-based gold electroplated electrodes 18

4.1.3 Microfabricated gold electrodes 18

4.2 Design consideration of interdigitated electrodes 18

4.3 Electrodes surface treatments 22

4.4 Measurements and data analysis 24

CHAPTER 5 IMPROVEMENT AND OPTIMIZATION 27

5.1 Cross linker for immobilization of protein probe 27

5.1.1 Reagents and samples 27

5.1.2 Performance of sensors with cross linker modification 28

5.2 Immobilization buffers 32

5.2.1 Reagents and samples 32

5.2.2 Sensor performance with various immobilization buffers 33

5.3 Testing buffers 35

5.4 Applied AC signal frequency and voltage 39

5.5 Summary of the sensing platform's performances 42

CHAPTER 6 VARIOUS APPROACHES FOR PATHOGENS DETECTION IN COMPLEX MATRICES 44

6.1 Influenza A virus 44

6.2 Protein (antibody to pseudorabies virus) 48

6.3 Nucleic acids RNA and DNA 48

6.3.1 Reagents 48

6.3.1 Zika virus RNA 50

6.3.3 HSV-1 DNA 57

CHAPTER 7 EXPANSION TO CHEMICAL DETECTION 60

7.1 Electrodes fabrication 60

7.2 Reagents and samples 63

7.3 Capacitance change with time during assay 63

7.4 Working condition optimization 65

7.5 Dose response 65

7.6 Specificity 68

7.7 Complex river samples 70

CHAPTER 8 CONCLUSONS AND FUTURE WORK 73

8.1 Conclusions 73

8.2 Future work 74

LIST OF REFERENCES 76

VITA 83

LIST OF TABLES

Table 1 Equivalent circuit fitting for gold electrodes on silicon wafer and copper PCB electrodes (Reactance calculated at 100 kHz). 21

Table 2 Summary of the sensing platform's performance on detecting various pathogens. 43

Table 3 Surface water samples detection and recoveries..... 71

LIST OF FIGURES

Figure 1 Configuration of an SPR device. SPR's wave-matching condition is very easily disrupted by even very tiny changes in the interface conditions.[45]..... 9

Figure 2 Equivalent circuit for a pair of sensor electrodes in fluid. 14

Figure 3 Commercially available Surface Acoustic Wave (SAW) electrode chip. 17

Figure 4 Copper-based gold electroplated PCB electrodes by chemical etching. 19

Figure 5 Gold Electrodes on silicon wafer. 19

Figure 6 Equivalent circuit fitting of (a) gold electrodes on silicon wafer and (b) copper electrodes fabricated by printed circuit board (PCB) etching. 19

Figure 7 A drop of deionized water (3 μL) on (a) pristine and (b) irradiated polyimide surfaces and (c) the irradiated polyimide surface after plasma treatment. (d) Electrodes with a mini-chamber and two Cu foil leads attached. (e) Sensor responses with different ozone surface treatments. 23

Figure 8 Cyclic voltammetry characteristics of sensor's (a) incubation and (b) blocking process..... 25

Figure 9 Response of 0.1×PBS, 4μg/uL BSA and 10 fg/mL, 100 fg/mL and 1 pg/mL goat anti-bovine IgG antibody samples on electrodes functionalized with probe, in addition to 100 fg/mL and 1 ng/mL goat anti-bovine IgG antibody samples on dummy electrodes coated with BSA. Inset is dose response of sensor electrodes without APTES modification. 29

Figure 10 Dose response of influenza A samples as a function of concentration. Tests conducted on electrodes modified with APTES chemical linker (black) yields a linear

correlation between sensor output and sample concentrations with an LOD of 0.2513 pg/mL. Tests conducted on electrodes treated with passive functionalization method (blue) demonstrates very small responses..... 31

Figure 11 Tests of 18.76×10^3 copies/μL Zika virus RNA sample are conducted on chips incubated with probes prepared in ultrapure water, 0.05×PBS and 1×PBS. Probes in 0.05×PBS is considered to be the optimal due to its high response. 34

Figure 12 Evaluation of sensor's performances when probe is prepared in 0.05×PBS and ultrapure water. Probe prepared in 0.05×PBS and DNA samples in 0.5×SSC (black) is the optimal immobilization buffer with an LOD of 0.986 pg/mL (6.38 copies/μL or 0.0106 fM). 36

Figure 13 Dose response of Zika RNA spiked in 0.5×SSC and 1×SSC for testing buffer evalution. 0.5×SSC is considered to be the optimal testing buffer and d|C|/dt is 2.40±0.50 %/min for 187.6 copies/μL (1 pg/mL), 5.19±1.12 %/min for 1,876 copies/μL (10 pg/mL) and 7.52±0.78 %/min for 18,760 copies/μL (100 pg/mL), showing a clear logarithmic dependence on Zika virus RNA. Its LOD in 0.5×SSC is yielded to be 0.986 pg/mL (78.825 copies/μL) with a response of 1.458 %/min..... 36

Figure 14 Evaluation of sensor's performances when HSV-1 virus DNA is prepared in 0.5×, 1× and 2×SSC. Probe prepared in 0.05×PBS and DNA samples in 0.5×SSC (black) is the optimal immobilization buffer with an LOD of 0.986 pg/mL (6.38 copies/μL or 0.0106 fM). 38

Figure 15 Responses of 0.1×PBS-T, 1.52 ng/mL influenza A virus on functionalized electrodes, and 152.5 ng/mL influenza A virus sample on dummy electrodes (a) when

using 10 mV AC signal with its frequency varied from 20 kHz to 200 kHz and (b)when using 100 kHz AC signal with its voltage varied from 5 mV to 100 mV. (c) Responses of 50, 500 and 5000 pg/mL HSV-1 virus DNA and 5000 pg/mL HSV-2 virus DNA. 40

Figure 16 Responses of clinical negative and positive swab samples of dilution factor of 1:100,000, 1:10,000 and 1:1,000. 45

Figure 17 Comparison of results from ACEK capacitive sensors and those from commercial tests for a blind panel test of influenza virus A from nasal swabs. (a) Responses of all tested samples differentiated by the -0.40 %·min^{-1} cut-off line (blue) and (b) correlation between PCR cycles and responses of samples determined as positive by ACEK capacitive sensor in blind tests. The strongest positive sample is the limit of a commercial rapid influenza test. 47

Figure 18 (a) Responses of FBS in different dilution rates. (b) Dose response of protein IgG in 1% serum matrix..... 49

Figure 19 Tests of pseudorabies virus clinical samples. Positive and negative samples can be clearly differenced..... 49

Figure 20 Responses of non-specific nuclei acid (HSV-1 and dengue) and virus (influenza A), and dose response of Zika virus RNA spiked in serum/lysing solution. 51

Figure 21 Responses of Zika virus RNA in lysing or GuSCN solution containing 1% serum by various probes. 53

Figure 22 Zika and Dengue virus RNA responses with various probes (Probe #1 and #2) and testing buffer containing pure serum: (a) Probe #1 with 1:1:1 of serum, GuSCN

and 2×SSC as testing buffer; (b) Probe #1 with 1:1 of serum and lysing solution as testing buffer; (c) Probe #2 with 1:1:1 of serum, GuSCN and 2×SSC as testing buffer; and (d) Probe #2 with 1:1 of serum and lysing solution as testing buffer. 56

Figure 23 Responses of tests on Probe #2 functionalized electrodes vs. Zika virus RNA concentration converted into pure serum. 56

Figure 24 Responses of DNA spiked serum diluted in lysing solution using different dilution factors. 58

Figure 25 Dose response of HSV-1 DNA serum samples with 1:20 and 1:10 dilution. .. 58

Figure 26 (a) Schematic illustration of the laser direct writing of electrode on a polyimide substrate, (b) Typical photo image of flexible electrodes, (c) SEM images of the porous carbonized structures and (d) Raman spectra of the polyimide regimes with and without laser irradiation. 61

Figure 27 The measured impedance spectra (solid line) of the electrode cell and its equivalent circuit fitting (dotted line). 64

Figure 28 Normalized capacitance changes of control, BPA, BPS and BPF samples with time. 64

Figure 29 Response of control and 1 fM BPA samples (a) when using 1 kHz AC signal with its voltage varied from 100 mV to 400 mV and (b) when using 300 mV AC signal with its frequency varied from 500 Hz to 10 kHz. 66

Figure 30 Detected dose response of BPA samples as a function of concentration by data obtained in (a) 20 seconds and (b) 10 seconds. 66

Figure 31 Illustration of sensor specificity. The blue line is the sensor response of LOD (58.28 aM)..... 69

Figure 32 Ultrasensitive capacitive sensors with directed movement of complex sample particles with applied the ACEO effect. 71

CHAPTER 1

INTRODUCTION

1.1 History, development and challenges of biosensor

The field of biosensor, in the past 60 years, has undoubtedly attracted a great amount of research and development efforts. Researchers and scientists from chemistry, physics, microbiology, as well as various disciplines of engineering have been deeply involved in this interdisciplinary field. In 1956, Professor Leland C. Clark publishes his monumental paper on the development of an oxygen probe using the enzyme glucose oxidase (GOX) in transducer in measurement of glucose. In 1962 he described how “to make electrochemical sensors (pH, polarographic, potentiometric or conductometric) more intelligent” by adding “enzyme transducers as membrane enclosed sandwiches”[1]. Professor Clark is the inventor of the Clark electrode, which a device used for measuring oxygen in blood, water and other liquids[2]. He is considered as the "father of biosensors" and the modern-day glucose sensor used daily by millions of diabetics is based on his research.

Biosensor today is either sophisticated, high-throughput laboratory machine capable of rapid, accurate and convenient measurement of complex biological interactions and components or easy-to-use, portable device for use by non-specialists for decentralised, in situ or home analysis. The former are expensive and the latter are mass produced and inexpensive.[3]

Expansion of human activities and process of globalization speed up the high pace of people’s life and engagement, as well as the spread of pathogens and their vectors.

Influenza, for instance, is a very common infectious disease. While it usually causes only mild illness, it can be life-threatening for infants, elderly and immunodeficient people. Worldwide, seasonal influenza is estimated to cause 250,000–500,000 deaths per year. Historically, influenza caused pandemic such as the Spanish flu pandemic of 1918. Recent years, worldwide human health has been challenged by pandemic threats such as the emergence of highly pathogenic influenza A virus from mutation of avian influenza or other animal reservoirs. It is well established that timely diagnosis of viral infection can shorten the delay in treatment, reduce the duration of hospitalization, and improve the quality of patient care. Recently, the potential health consequences of Zika virus infection, and the lack of effective treatment for the disease, the World Health Organization (WHO) declared a public health emergency and released a call for the development of new diagnostic tests for Zika virus infection. Zika virus is a flavivirus (family Flaviviridae) that was first identified in Nigeria in 1947.[4] Many people infected with Zika virus were either asymptomatic[5] or reported having only mild, nonspecific influenza-like symptoms, such as fever and headache. Most patients typically recover within several days to a week.[6] However, the viral infection occasionally causes severe manifestations, including Guillain-Barre syndrome, in adults and microcephaly in babies when the mother has been infected with the virus during pregnancy. There also has been increasing concerns regarding the potential risk of sexual transmission of Zika virus during pregnancy.[7] Therefore, a rapid point of care (POC) diagnosis for infectious diseases outside hospital is desired and will have significant impact on the healthcare.

Despite for the area of infectious diseases detection, recent years have also seen a growing need to monitor and rapidly detect contaminants in the environment and food supply such as bisphenol A (BPA). BPA is a monomer widely used in a variety of consumer products, including plastics, food packaging, dental sealants, and thermal receipts. It was reported that 8-15 billion pounds of the material were produced annually[8]. Because of the widespread use of BPA, the compound has been detected in aquatic environments, which are considered the ultimate reservoirs for environmental anthropogenic chemicals. BPA is a known endocrine disruptor with estrogenic, antiandrogen properties and can disrupt thyroid function. Studies have demonstrated that BPA can have significant biological effects at low, environmentally relevant doses[9],[10]. Significant levels of BPA have been detected in river water, river sediments, and fish muscles. In particular, there is concern that the consumption of fish could contribute to the total intake of BPA in human populations. Detection and quantification of BPA concentrations in water are critical for the U.S. Environmental Protection Agency to develop water quality standards and to evaluate environmental risk levels for the protection of human health. The majority of current BPA detection methods rely on high performance liquid chromatography (HPLC) or enzyme-linked immunosorbent assay (ELISA), which require the use of costly instruments by skilled personnel with complex and time-consuming operation[11]. Therefore, a simple and affordable method to monitor BPA level in environmental samples with high sensitivity remains critical.

Similar to the need of simple and easy-to-use method to detect BPA, interest of developing detection method of influenza is also growing. Currently, accurate diagnosis of

influenza virus is done by either virus isolation, detection of virus-specific antibodies or genomic detection by reverse-transcription polymerase chain reaction (RT–PCR). Virus isolation and antibody tests take several days and can hardly meet the time-sensitive needs of patient management. Real-time RT–PCR-based molecular assays can yield results in hours and are being increasingly used for early diagnosis. However, real-time RT-PCR requires good financial and technical resources to perform, often restricted to central laboratories.

1.2 Improvement on capacitive sensing

Previously, our group has developed an AC electrokinetics-based capacitive sensing method with microfabricated interdigitated electrodes that could reach a limit of antigen-antibody detection of 10 ng/ml. With adoption of cross linker during electrodes functionalization and studies on immobilization and testing buffers, the limit of detection (LOD) are improved significantly to pg/mL level and the sensing platform is expanded to nucleic acid and chemical detections. In addition, by researches on the various designs of electrodes, compatibility of ACEK sensing method was studied to support rapid and low cost prototyping and manufacturing, and AC electroosmotic effect is also utilized for capacitive sensing, expanding the varieties of ACEK capacitive sensing.

CHAPTER 2

LITERATURE REVIEW

The clear and enormous need for healthcare and environmental monitoring continues to drive substantial research in the field of biosensor. The last three decades have witnessed the remarkable development and progress of sophisticated and accurate traditional laboratory based sensing instrumentations. Although both high throughput sensing in traditional laboratory based sensing instrumentation and of low cost sensing for field or personal use are highly demanded, the need for low cost sensing for healthcare and environmental monitoring, for example, has particular benefit to developing economies, in particular within Africa and South East Asia[12]. There are special needs for low-cost point-of-care (POC) diagnostic and monitoring tools due to the lack of suitable testing clinics and facility. Additionally, while considerable research effort has been devoted to biosensors for diagnosis at the bedside or in the clinic, there have been few successful devices being routinely used in real applications.

While considerable research effort has been devoted to biosensors for diagnosis at the bedside or in the clinic, there are few successful POC devices being routinely used in real applications. POC diagnostic systems require the following critical attributes: sufficient sensitivity, robustness, simple test procedure and short sample-to-result time. Recent progress in the development of such systems has been fueled by rapid innovations in microfluidics, miniaturization, and enhanced signal detection technologies. Current POC diagnostics, based primarily on immunoassay technologies, have been the mainstream application for decades. However, traditional immunoassay technologies are not very

sensitive and need a long time to yield result, which limits the applicability of these tests to many clinical conditions. The obstacle to achieving rapid detection is the long diffusion time for the target bioparticles to reach the sensing site of a sensor. So accelerating the diffusion process has been an essential part of the study. Most of the reported biomolecular sensors work with heavily processed samples, requiring purification, pre-concentration, etc. in addition to sophisticated data processing and expensive equipment. Another challenge is specificity. A number of ultrasensitive immunosensing methods have been developed, many based on nanotechnology. However, only a few of the newer ultrasensitive methods have been evaluated with real patient samples, which is key to establishing clinical sensitivity and selectivity.

2.1 Electrochemical enzymatic biosensors

Electrochemical biosensors have traditionally received the major share of the attention in biosensor development[13]. Due to the simple, inexpensive and yet accurate and sensitive platform electrochemical biosensors have provided, they have always been a major role in the move towards simplified testing, including home-use devices[14]–[17].

Being capable of mass production with low cost and adequate accuracy and sensitivity are major criteria for successful commercialization of POC sensors and devices. Categorized as amperometric sensors, the electrochemical glucose sensors have attracted the most attention due to the sensors' unbeaten sensitivity and selectivity, even though numerous processes and methodologies have been developed for creating new glucose biosensors such as electrochemical methods[18], colorimetry[19], conductometry[20], optical methods[21], and fluorescent spectroscopy[22]. The portable glucose biosensors

which only requires a 0.3- to 1.5-μL drop of blood and usually take less than 10 seconds for the result have achieved the most significant commercial success[23]. Amperometric biosensors function by the production of a current (typically in nA to μA range) when a potential is applied between two electrodes.

2.2 Labeled affinity biosensor

Affinity biosensor measures the affinity between bioreceptors and target analyte, and labledeed affinity biosensor uses label molecular to help detect the target. For example, fluorescence labeling[24],[25], radiolabeling or isotope labeling, etc. Introducing microfluidics into POC systems attracts increasing interest and offers new ways and methods for POC diagnostics[26]. ELISA (enzyme-linked immunosorbent assay)[27] is a plate-based assay technique designed for detecting and quantifying substances such as peptides, proteins, antibodies and hormones. A detection enzyme or other tag can be linked directly to the primary antibody or introduced through a secondary antibody that recognizes the primary antibody. Detection is accomplished by assessing the conjugated enzyme activity via incubation with a substrate to produce a measurable product. Since the traditional ELISA relies on diffusion of the reactants to the antibodies immobilized on the microwell surface, the incubation times can be as long as a few days per assay. A strategy to reduce the assay time lies in reducing the well volume while increasing its surface area, which leads directly to miniaturization and microfluidic integration[28]–[34]. Microfluidics can improve the sensitivity, speed, and reduce costs of an immunoassay over ELISA by overcoming the issues of the large sample volume, long assay duration and low sensitivity. By employing a bead-based immunoassay in a microfluidic channel, Sato et al.

reported to shorten an immunosorbent assay overall time from 24 hr to less than 1 hr with a limit of detection of 1 µg/ml[35]. To lower the cost of the sensing platform, Microfluidic Paper-based Analytical Devices (µPADs)[36], [37] is another option. Paper itself has advantages like being inexpensive, flexible, light weight, disposable, compatible with biological samples, and can be easily modified by chemicals. Since capillary force in wet paper could be the mainly driving force for fluids flow delivery, complicated supporting pump is not necessary. This allows biosensors to be more readily transformed in lab-on-a-chip with capillary microfluidics[38]. Nevertheless, drawbacks like low limit of detection and sensitivity, immaturity of paper based devices and losing activity of bioreceptors with time limit the application of µPADs.

2.3 Label-free affinity biosensors

Labeled biosensors require a label attached to the target for signal amplification purposes and during readout the amount of label is detected and assumed to correspond to the number of bound targets. However, steps such as labeling a biomolecule would increase the complexity and time of sensor operation, drastically change its binding properties, and the yield of the target-label coupling reaction can be highly variable[39]. Being label-free, thus eliminating the need for labeling (fluorescent, chemical, or radioisotope) target molecules, is important.

Surface plasmon resonance (SPR)[40],[41] based label-free biosensor can be utilized to detect bioparticles reactions such as protein binding[42],[43] and hybridization of different types of nucleic acids[44]. Figure 1[45] shows the configuration of an SPR device. The surface plasmons (SPs) is a free charge oscillation that exist at the interface

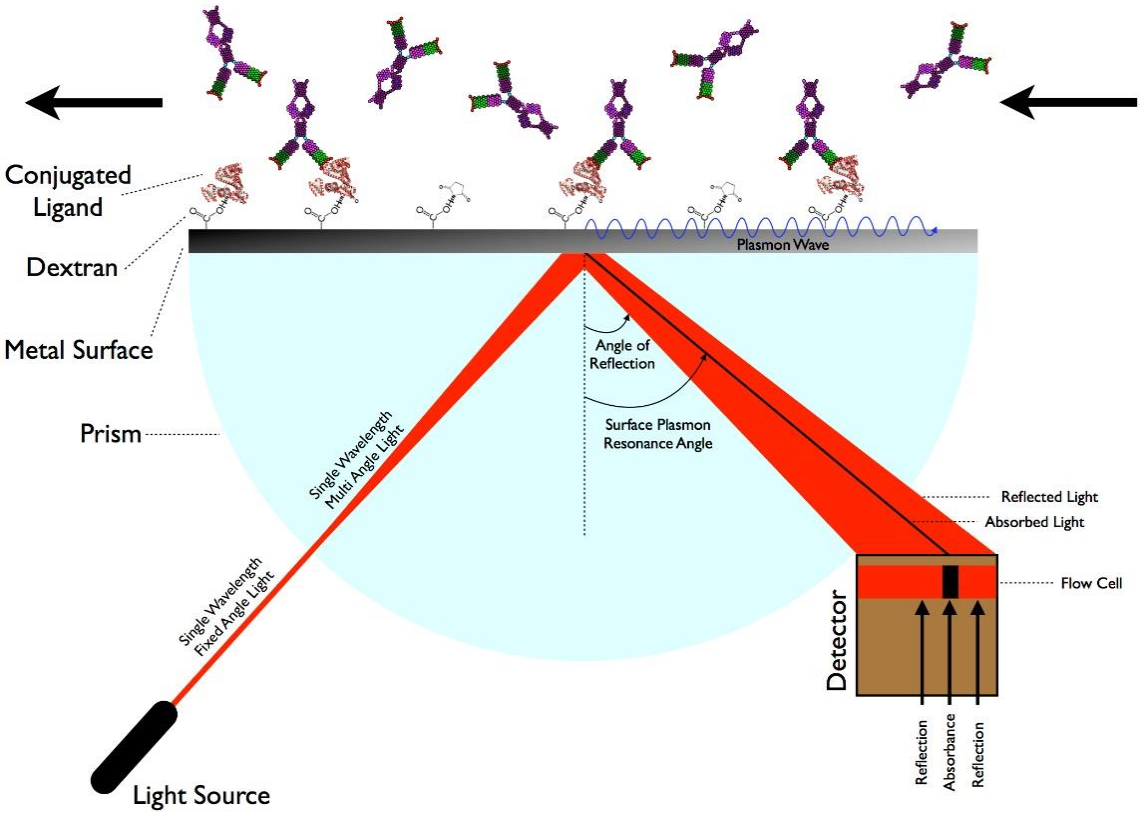

Figure 1 Configuration of an SPR device. SPR's wave-matching condition is very easily disrupted by even very tiny changes in the interface conditions.**[45]**

between any two materials[46]. A fraction of the light energy incident at a sharply defined angle can interact with the delocalized electrons in the metal film (plasmon) thus reducing the reflected light intensity. In Figure 1, a single wavelength laser beam enters a prism which results in many light angles striking the metal surface, all of them are reflected except for the angle in which the metal will absorb and turn its energy into a plasmon wave onto its outer surface, at this angle no light is reflected and thus appears with very little intensity on the detector. Since the plasmon wave propagates on the outer side of the metal, any interaction with the conjugated protein will change the resonance angle[45]. The SPR biosensors have been widely applied in a diverse range of fields, including molecular recognition, and disease immunoassays, etc.[47]–[52]

Impedance spectroscopy is another example of label-free strategy for transducing biological recognition events[53]. It has been widely used for probing various types of biomolecular interactions such as immunosensors, DNA hybridization, rapid biomolecular screening, cell culture monitoring, etc.[54]–[57], since Newman and Martelet[58] who come up with the concept of impedimetric based immunosensors. So far, impedimetric immunosensors have been successfully applied at the academic level. However, no prototypes have been released into the market and this fact has brought the reliability of them into question.

CHAPTER 3

AC ELECTROKINETICS

ACEK effects, including dielectrophoresis (DEP), ACEO and ACET effects, are increasingly used in microfluidic devices to manipulate fluids and embedded objects[59]. DEP directly acts on the particles embedded in the fluid, while ACEO and ACET effects induce fluid movements that carry the embedded particles. ACEK effects improve the sensor sensitivity and response time by accelerating the travel of target molecules to the electrode surface[25],[60],[61].

3.1 Dielectrophoresis

Dielectrophoresis, or DEP, refers to the interaction between a dipole moment on a particle and a non-uniform field[62]. This technique has been studied in great details for controlled manipulation of particles, binary separation, and characterization of particles. The DEP force on a spherical particle can be described as followed[63],

$$F_{DEP} = \pi\varepsilon_m a^3 \mathrm{Re}\left[\frac{\varepsilon_p^* - \varepsilon_m^*}{\varepsilon_p^* + 2\varepsilon_m^*}\right]\nabla|E|^2 = \pi\varepsilon_m a^3 \mathrm{Re}[K(\omega)]\nabla|E|^2 \quad (3.1)$$

where ε_m is the medium permittivity, a is the radius of the particle, ε_p^* and ε_m^* are particle and medium complex permittivity respectively.

Complex permittivity is defined as $\varepsilon^* = \varepsilon - j\frac{\sigma}{\omega\varepsilon}$ (σ: conductivity; ω angular frequency). $K(\omega)$, a function of ω, is also known as Clausius–Mossotti factor. Therefore, the DEP force F_{DEP} is frequency dependent. In the context of electrokinetic manipulation, the real part of the Clausius–Mossotti factor is a determining factor for the dielectrophoretic force on a particle. For $\mathrm{Re}[K(\omega)] > 0$ (or < 0), $F_{DEP} > 0$ (or < 0) and positive (or

negative) DEP will be applied on the particle. Since positive DEP force on a particle traps the particle at the surface of electrodes while negative DEP repels the particle away from the electrodes, in this work, positive DEP would be applied to accelerate the binding reaction between virus and antibody. As is shown in Equation 3.1, F_{DEP} depends on the particle volume. For nanoscale macromolecules, DEP may not be effective unless the molecules are located within a very short distance to the electrodes (<1 mm).

3.2 AC Electroosmosis

ACEO effect can induce microfluidic vortices above electrodes to transport target molecules to the electrode surface for binding[64]–[67], which improves the detection sensitivity and response time. ACEO typically dominates at low ionic strengths, such as target samples diluted in water. But the flow velocity of ACEO has been observed to decrease significantly with increasing conductivity and eventually drop to zero above 0.085 S/m[68]. Hence for medical and biological applications involve the use of solution with high conductivity the ACEO flow will be negligible. ACEO flows are caused by the movement of induced charges in the EDL at the solid-liquid interface when a non-uniform AC electric field is applied. The induced counter-ions will move under a tangential electric field to generate ACEO flows. ACEO fluid velocity is approximately given as

$$u_{ACEO} = -\frac{\varepsilon_m}{\eta} \cdot \Delta\xi \cdot E_t \tag{3.2}$$

where $\boldsymbol{\varepsilon_m}$ and $\boldsymbol{\eta}$ are the permittivity and viscosity of the medium, $\boldsymbol{E_t}$ is the component of the electric field strength tangential to the electrode surface, and $\boldsymbol{\Delta\xi}$ is the voltage drop over the interfacial layer including the EDL and molecular deposition at the electrode surface[63]. ACEO velocity is known to exhibit a bell-shaped dependence on frequency

due to the charging process of EDL. Therefore, the frequency of capacitive sensing needs to be optimized to maximize ACEO effect.

3.3 AC electrothermal effect

ACET effect arises from uneven Joule heating due to an electric current flowing through the fluid. Once the AC electric field is applied in the bulk solution, polarized particles would be separated and migrate, which generates the ionic current. The time average electric thermal force is shown in Equation 3.3,

$$F_{ET} = -0.5\left[\left(\frac{\nabla\sigma}{\sigma} - \frac{\nabla\varepsilon}{\varepsilon}\right) E \frac{\varepsilon E}{1+(\omega\tau)^2} + 0.5|E|^2\nabla\varepsilon\right] \quad (3.3)$$

where E is the electric filed strength, ω is the frequency of the applied excitation, ε and σ are medium permittivity and conductivity respectively, $\tau = \varepsilon/\sigma$ is the charge relaxation time.

Separation of the electrodes used in our tests is around 2 um, which leads to a quite low ACET force that can also be neglected. As a result, the only dominated force for target virus concentration is the DEP force, which is calculated to be $2.25\times10^{-17}N$, leading to a fluid velocity of $47.5\mathrm{nm/s}$.

3.4 Capacitive sensing

When immersed into fluid, the interdigitated electrode cell can be electrically represented by an equivalent circuit. The circuit shown in Figure 2 consists of the electrode's self-resistance (R_{wire}), interfacial capacitance (C_{int}), charge transfer resistance (R_{ct}), solution bulk resistance (R_s) and dielectric capacitance of the electrode cell (C_s). The interfacial capacitance is a combination of electric double layer (EDL) and deposited

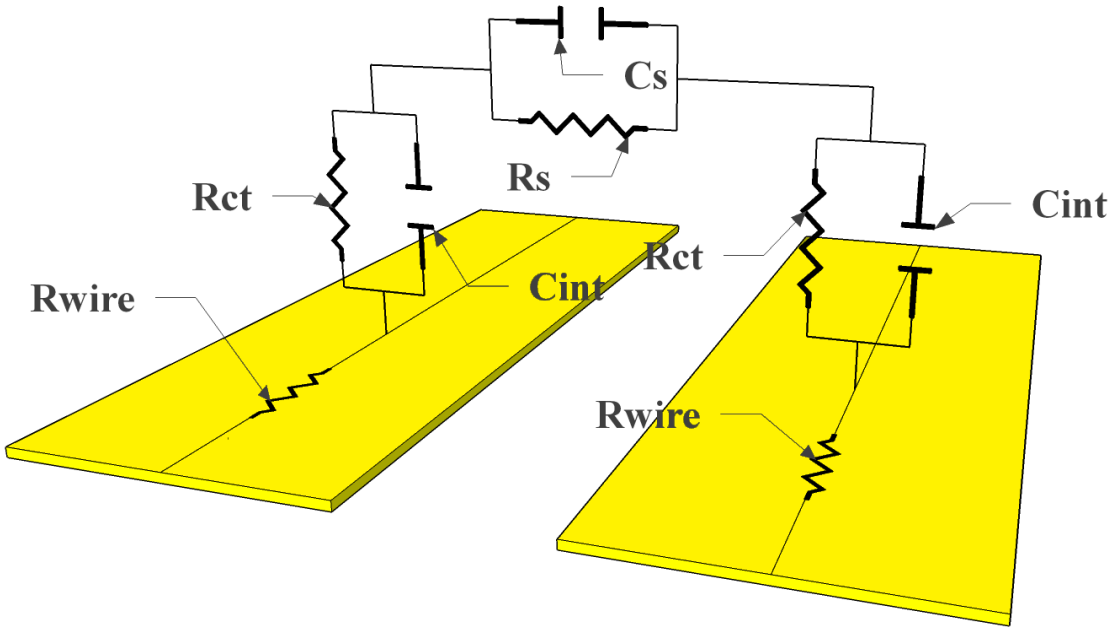

Figure 2 Equivalent circuit for a pair of sensor electrodes in fluid.

bioparticles capacitance and is expressed as in Equation 3.4,

$$C_{int} = A_{int} / \left(\frac{1}{\varepsilon_p} d_p + \frac{1}{\varepsilon_s} d_{edl} \right) \quad (3.4)$$

where A_{int} is the surface area of the interfacial capacitor of the functionalized electrode, d_p and d_{edl} are the thickness of bioparticle immobilized and electric double layer formed on the electrodes surface respectively, ε_p is the bioparticle permittivity and ε_s is the solution permittivity. When bioparticles are immobilized on the surface and binding reaction occurs, d_p will increase and therefore result to the interfacial capacitance to reduce.

CHAPTER 4

ELECTRODES FOR DIRECT CAPACITIVE BIOSENSING

The sensing platform in this work is based on AC electrokinetics (ACEK) capacitive sensing technology.[69] It adopts low cost interdigitated microelectrodes functionalized with a capture bioreceptor targeting the pathogen bioparticles that need detection. During the assay, an AC signal is applied onto the microelectrodes to induce microfluidic phenomena by ACEK effects that cause targets in the sample solution applied on electrodes to move towards the electrode surface and bind with the immobilized bioreceptor. The binding causes a change in the interfacial capacitance (C_{int}) at sensor surface, and is detected electrically using the same ACEK signal.

4.1 Various interdigitated electrodes

4.1.1 Surface acoustic wave (SAW) resonators

The Surface Acoustic Wave (SAW) electrode chips used in our ACEK capacitive assay are modified from AVX Corps' PARS 433.92 chip. The metal cover of the SAW resonator is removed mechanically to expose the working electrode array for use, as shown in Figure 3. The detection surface consists of aluminum electrodes deposited on quartz substrate. Each electrode finger is 2.0 μm wide, 170μm long, with 1.5 μm spacing from each other. The metal housing around the electrode chip is about 4mm (L) x 2.5mm (W) x 1mm (H), and accommodates ~10μL of sample. The interdigitated electrodes are electrically connected to two contact pads on the chip bottom, which are then connected to an impedance analyzer (Agilent 4294A).

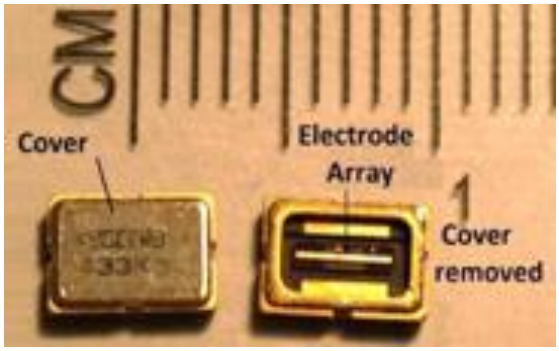

Figure 3 Commercially available Surface Acoustic Wave (SAW) electrode chip.

4.1.2 Copper-based gold electroplated electrodes

The copper-based gold electroplated printed circuit board (PCB) electrodes shown in Figure 4 are fabricated by chemical etching method. Electrode finger is 400 μm wide and 200 μm in separation. Pattern of electrodes is printed on toner transfer paper in ink and then transferred onto the copper sheet by using laminator whose temperature is set to be 379°F. After being slipped into water to release the paper from image picture, the board is cleaned and dried, toner reactive foils are applied to seal the toner image against the etchant, resulting in a perfectly etched image. With the ink sealed and protected by toner reactive foils, the patented copper sheet is then immersed into copper etchant, or ferric chloride (MG Chemicals), which is heated to 55°C (135°F). After etching the board, toner reactive foils and underlying toner are removed by wiping down the board with Acetone.

4.1.3 Microfabricated gold electrodes

Microfabricated gold electrodes shown in Figure 5 are using lift-off method. 30 nm gold layer is deposited on the 10 nm chromium adhesion layer and then the 500 nm silicon dioxide layer. Each gold electrode finger is 4 μm wide and 4 μm spacing in between each other.

4.2 Design consideration of interdigitated electrodes

The suitability of an IDE can be evaluated by extracting the equivalent circuit of the IDE. Figure 6 shows the fitting of gold electrodes on silicon wafer and copper PCB electrodes. A Warburg (Z_w) is added in series with R_{ct} in Figure 2 to represent the diffusion effect in EDL for a better fitting of the circuit at low frequency. Fitted values are listed in

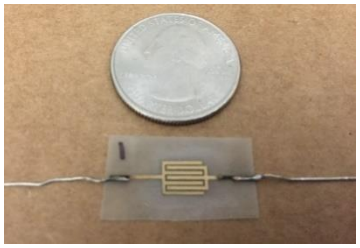

Figure 4 Copper-based gold electroplated PCB electrodes by chemical etching.

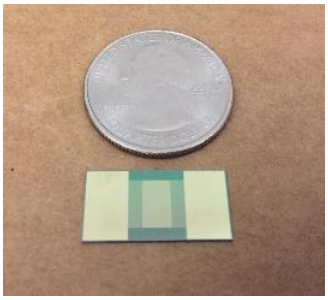

Figure 5 Gold Electrodes on silicon wafer.

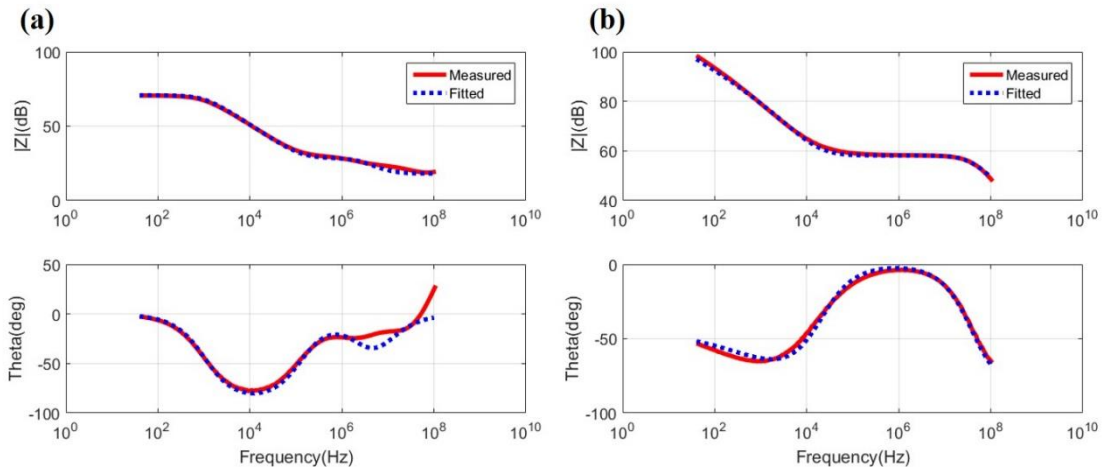

Figure 6 Equivalent circuit fitting of (a) gold electrodes on silicon wafer and (b) copper electrodes fabricated by printed circuit board (PCB) etching.

Table 1, from which it can be seen that for the gold electrodes on silicon wafer, C_s and C_{int} are comparable and both in nF level.

At the experimental frequency, which is 100 kHz, the circuit is expected to be simplified into C_{int} in series with R_s only. In order to achieve that, $X_{Cint} << X_{Rct+Zw}$ and $X_{Cs} >> R_s$ are expected. From the calculated reactance values listed in Table 1, for gold electrodes on silicon wafer, X_{Cs} is not as greater than R_s as that of PCB copper electrodes. Therefore, as what has been justified by experiments, gold electrodes showed quite poor response that cannot correctly be associated with the occurrence of binding reactions. To satisfy $X_{Cint} << X_{Rct+Zw}$ and $X_{Cs} >> R_s$, C_{int} is required to be much greater than C_s. Expression of C_{int} is given in Equation 3.4. Similarly, Cs is shown as follows:

$$C_s = A_{electrodes} \Big/ \left[\frac{1}{\varepsilon_s}\pi\left(\frac{g}{s} + \sigma w\right)\right] \tag{4.1}$$

where $A_{electrodes}$ is the electrodes area, g and w are the electrodes digit gap and width separately, and σ, which is usually equal to 20%, is the percentage of the electrodes digit width that is included in C_s. The C_{int}/C_s ratio can then be estimated as follows by recalling Equation 3.4:

$$\frac{C_{int}}{C_s} = \frac{A_{int}/\left(\frac{1}{\varepsilon_p}d_p + \frac{1}{\varepsilon_s}d_{edl}\right)}{A_{electrodes}/\left[\frac{1}{\varepsilon_s}\pi\left(\frac{g}{s}+\sigma w\right)\right]} = \frac{wl/\left(\frac{1}{\varepsilon_p}d_p + \frac{1}{\varepsilon_s}d_{edl}\right)}{\frac{wl}{2}/\left[\frac{1}{\varepsilon_s}\pi\left(\frac{g}{2}+\sigma w\right)\right]} = \frac{\pi(g+2\sigma w)}{d_p + d_{edl}} > 10^3 \tag{4.2}$$

where l is the electrodes digit length. Since the EDL thickness and bioparticle in real samples are both usually less than 100 nm, by using electrode in hundreds of micrometers would result in the C_{int}/C_s ratio to be as high as 10^3, which also offers explanation as to why gold electrodes on silicon wafer showed worse output response than the copper PCB electrodes.

Table 1 Equivalent circuit fitting for gold electrodes on silicon wafer and copper PCB electrodes (Reactance calculated at 100 kHz).

Element	Silicon Wafer [Gold]	PCB [Copper]
R_{wire}	5 Ω	8 Ω
R_{ct}	3400 Ω	36 Ω
Z_w	100 Ω·S-0.5	1.3 MΩ·$S^{-0.5}$
X_{Rct+Zw}(calculated)	**3.4 kΩ**	**1.666 kΩ**
C_{int}	35 nF	20nF
X_{Cint}(calculated)	**45.47 Ω**	**79.57 Ω**
R_s	18 Ω	800 Ω
C_s	3.3 nF	5.1 pF
X_{Cs}(calculated)	**482 Ω**	**0.31 MΩ**

4.3 Electrodes surface treatments

For the metal electrodes such as SAW chips and copper PCB electrodes, prior to incubation with linker and probe molecules, the microelectrode chips is thoroughly cleaned by washing with acetone, isopropyl alcohol and deionized water, and then treated with ozone or plasma. The surface quality is closely monitored by measuring the C_{int}. As for the laser printed electrodes, due to the multiscale morphology of the irradiated polyimide surface, wetting properties of interfacial capacitance sensors have become particularly important. The static contact angle of untreated polyimide is found to be 79±1° (Figure 7(a)), consistent with previous reports[70]. After laser ablation, the contact angle is increased to 99±1° (Figure 7(b)). Based on the microstructure characterization, this hydrophobicity can be attributed to both the carbonization and porous surface structure.

However, in most cases this hydrophobic character is not desirable for sensors, especially for detection in an aquatic medium. Plasma treatment is a good method for increasing the surface hydrophilicity by creating OH dangling bonds and enriching O^- ions on the surface without influencing the electrode microstructure characteristics. After 10 minutes of vacuum plasma treatment (PLASMA ETCH PE-50), the water drop completely infiltrates into the electrode surface (Figure 7(c)), indicating a marked surface transition from hydrophobicity to hydrophilicity. Besides plasma treatment, ozone treatment can also improve the hydrophilicity of the electrode surface by enriching O^- ions on the surface. So three types of surface treatments are investigated, including ozone at 15 min, 30 min and plasma at 5 min.

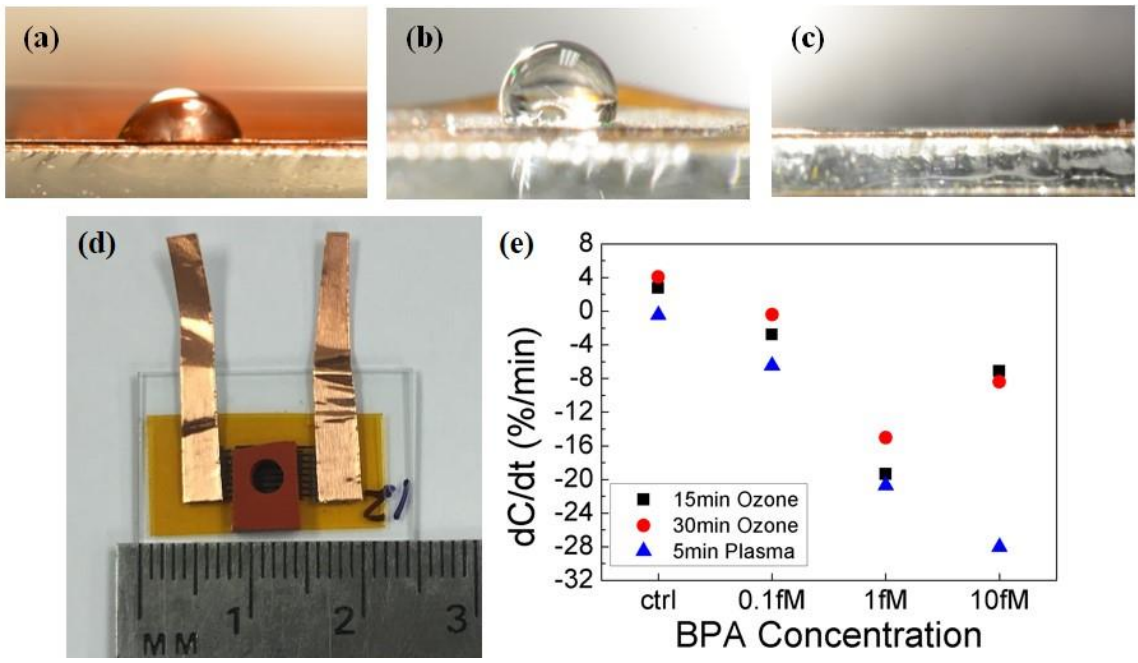

Figure 7 A drop of deionized water (3 μL) on (a) pristine and (b) irradiated polyimide surfaces and (c) the irradiated polyimide surface after plasma treatment. (d) Electrodes with a mini-chamber and two Cu foil leads attached. (e) Sensor responses with different ozone surface treatments.

The ultimate criterion of surface treatment for biosensor is to obtain sensitive response. So BPA samples at concentrations of 0.1 fM, 1 fM and 10 fM are applied to the sensors. The sensor response for each treatment is shown in Figure 7(e). It can be seen that the plasma treated sensors consistently have higher response than ozone treated sensors, regardless of treatment time. This means that the immobilization efficiency of sensors treated with plasma is improved since more aptamer attached to the electrode surface made the surface less likely to become saturated (responses to 10 fM BPA showed significant difference between plasma and ozone treated sensors). In conclusion, the plasma treated sensor exhibits large responses even in the limit of high PBA concentration, yielding a combination of high sensitivity and large dynamic range.

The electrode's functionalization after plasma treatment includes receptor incubation and uncovered surface blocking. As the incubation and blocking processes progressed, an increasing number of molecules become attached to the electrode surface. The quality of electrode functionalization is monitored by measuring the C_{int}. This method is validated in our prior work **[71]**. During the incubation and blocking process, C_{int} values have reduced by -58.05±3.19% and -93.35±2.06% respectively for BPA, indicated adequate molecular immobilization on the electrode surface. Surface immobilization reduces the current flowing through the electrodes, effectively increasing the charge transfer resistance, R_{ct}. Therefore R_{ct} is also measured during the incubation and blocking, which showed an increasing R_{ct} with time as shown in Figure 8.

4.4 Measurements and data analysis

This work uses ACEK-based capacitive sensing to monitor the molecular

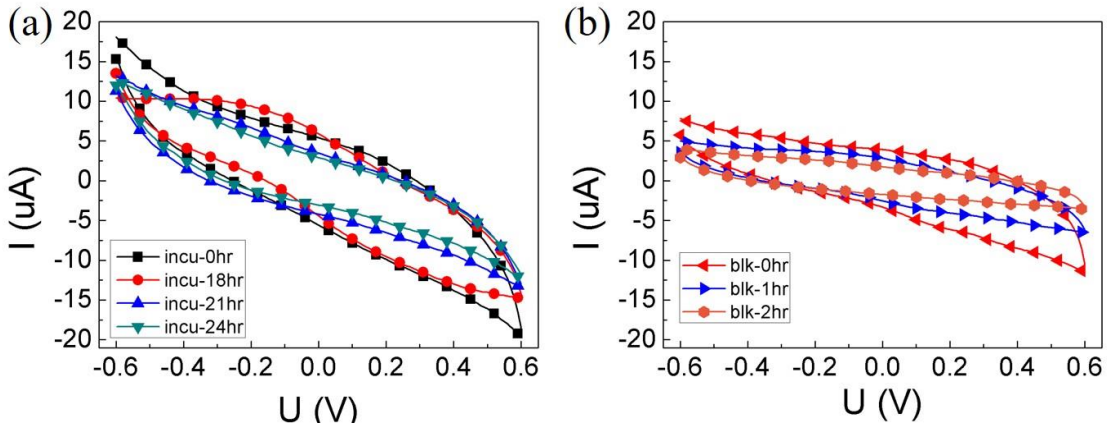

Figure 8 Cyclic voltammetry characteristics of sensor's (a) incubation and (b) blocking process.

deposition at the electrolyte/electrode interface. Prior work demonstrates that interfacial capacitance (C_{int}) can effectively detect molecular deposition on the electrode surface with high sensitivity and specificity[69],[72],[73]. In ACEK capacitive sensing, C_{int} is found by measuring the sensor cell's impedance at a fixed AC frequency and voltage continuously during the testing. The interfacial capacitance of the electrodes is sampled and recorded periodically by an Agilent 4294A impedance analyzer for 20 seconds. Then the percentage change, *dC/dt* in %/min, of the measured capacitance is adopted as the readout of the sensor, indicating the binding reaction occurring on the electrodes surface. Least square linear fitting algorithm is performed to determine the capacitance change rate.

CHAPTER 5

IMPROVEMENT AND OPTIMIZATION

5.1 Cross linker for immobilization of protein probe

5.1.1 Reagents and samples

5.1.1.1 Protein IgG

Sample solution uses 0.1×PBS (1 mM phosphate-buffered saline [pH 7.0] containing 15 mM sodium chloride) with a conductivity of 0.15–0.16 S/m (600–700 Ω·cm) as standard buffer for sample diltuion. 1mg/mL KKKKKAAAC cross linker is prepared by adding 1.2 mg KKKKKAAAC cross linker (New England Peptide, Gardner, MA) into 1.2 mL ultrapure water. The probe used for electrodes functionalization is 10 µg/mL bovine IgG whole molecule, which is 1:1000 dilution of 10 mg/mL bovine IgG whole molecule (Johnson ImmunoResearch, West Grove, PA) in ultrapure water. 1×10^{1} to 1×10^{6} fg/mL goat anti-bovine IgG antibody samples are obtained by diluting 2 mg/mL goat anti-bovine IgG antibody (Johnson ImmunoResearch) with 0.1×PBS. 100 µg/mL lactoalbumin is used for blocking, which is 1:10 dilution of 1mg/mL lactoalbumin (Sigma-Aldrich, St. Louis, MO) stock solution in ultrapure water. 4 µg/mL BSA, or bovine serum albumin protein, is prepared as interference by adding 40 µg BSA (Sigma-Aldrich, St. Louis, MO) in 10 mL 0.1×PBS.

5.1.1.2 Influnza A virus

Sample solution in this work is prepared using the same 0.1×PBS and 0.1×PBS-T as described for protein detection tests. 0.1×buffer B is 0.1×PBS-T containing 10 v/v%

SuperBlock (Pierce Biotechnology, Rockford, IL) and is used as the blocking reagent. The chemical linker used for improving surface functionalization with antibody is 10 v/v% 3-aminopropyltriethoxysilane (APTES, Thermo Scientific, Waltham, MA) in absolute ethanol and 2.5% glutaraldehyde in water. Antibody solution used for electrodes functionalization is 41.5 µg/mL anti-influenza A antibody in distilled water.

Antibody for electrodes functionalization is 1:100 dilution of 4.15 mg/ml anti-influenza A antibody (gift from a company) in distilled water to a concentration of 40 µg/ml. Antibody for dummy electrodes is 40 µg/ml bovine IgG whole molecule (Code# 001-000-003, Johnson ImmumoReserch, West Grove, PA), diluted from 10 mg/ml in distilled water. Spiked Influenza A virus sample is 1:100, 1:1,000 and 1:10,000 dilution of 0.1525 mg/ml influenza A virus (a gift from a company) in 0.1×PBST to concentrations of 1.525 µg/ml, 0.1552 µg/ml and 0.01525 µg/ml.

5.1.2 Performance of sensors with cross linker modification

As shown in Figure 9, 10 fg/mL, 100 fg/mL and 1 pg/mL goat anti-bovine IgG antibody spiked in 0.1×PBS are tested. Each concentration is tested in triplicate and their results are -3.07±0.59 %/min (10 fg/mL), -6.08±0.47 %/min (100 fg/mL) and -11.17±1.07 %/min (1 pg/mL), while the responses of the buffer solution 0.1×PBS and non-specific interference 4 µg/uL BSA are -0.10±0.46 %/min and 0.099±0.44 %/min respectively. Dummy electrodes coated with 4 µg/uL BSA are also tested with 100 fg/mL and 1 ng/mL goat anti-bovine IgG antibody samples, which show very small responses (-0.47±0.71 %/min and -1.13±0.46 %/min) compared with functionalized electrodes, indicating that the responses from active sensors are indeed due to the binding between the probe and the

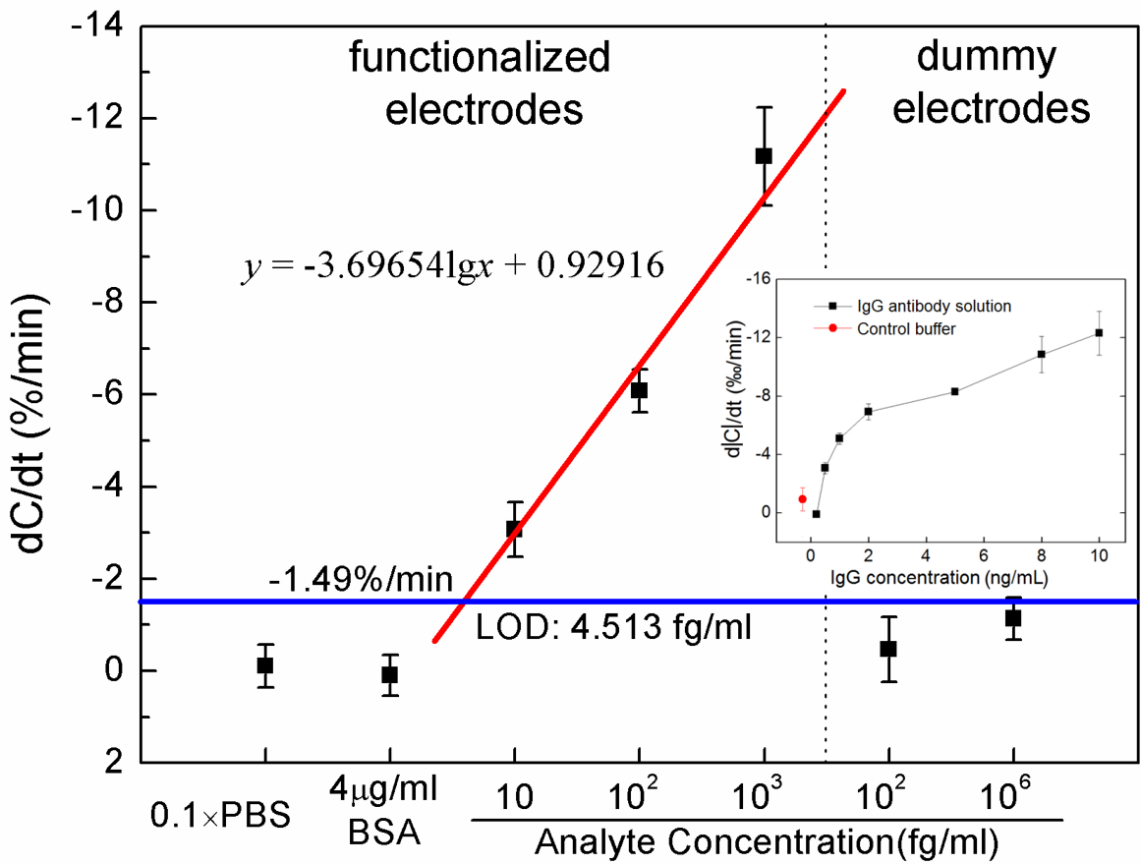

Figure 9 Response of 0.1×PBS, 4μg/uL BSA and 10 fg/mL, 100 fg/mL and 1 pg/mL goat anti-bovine IgG antibody samples on electrodes functionalized with probe, in addition to 100 fg/mL and 1 ng/mL goat anti-bovine IgG antibody samples on dummy electrodes coated with BSA. Inset is dose response of sensor electrodes without APTES modification.

analyte. The dependence of *dC/dt* on analyte concentration is approximated by linear fitting as $y = -3.69654 \cdot \lg x + 0.92916$ where x is the analyte concentration in fg/μL and y is the capacitance change rate, $d|C|/dt$, in %/min. The LOD is defined as 3 standard deviations from the response of the background control. Because the background produced a response of -0.10±0.46 %/min, the cut-off $d|C|/dt$ is calculated to be -1.49 %/min, which corresponds to 4.513 fg/mL goat anti-bovine IgG antibody. Dose response of electrodes without APTES modification is investigated in previous work[73], and it is shown in the inset of Figure 9. The responses are quite small and the data points are in ‰/min instead. In the tests with electrodes functionalized with passive adsorption of probe protein, the IgG antibody concentration ranges from 0.2 ng/mL to 10 ng/mL, and the tests of every IgG antibody concentration are also repeated three times using a new electrode each time. The responses for IgG antibody samples are -0.02±0.13 ‰/min at 0.2 ng/mL, -3.07±0.38 ‰/min at 0.5 ng/mL, -5.09±0.38 ‰/min at 1 ng/mL, and -6.93±0.56 ‰/min at 2 ng/mL respectively. Using an AC signal of 1 V_{rms} AC voltage with a duration of 10 min, an LOD of around 1 ng/mL is reached.

Dose response of influenza A virus samples in various concentrations (15.25 pg/mL, 152.5 pg/mL, 1.525 ng/mL, 15.25 ng/mL and 152.5 ng/mL) is shown in Figure 10. Tests are firstly conducted on the electrodes functionalized with bioreceptors by passive adsorption (i.e. without chemical linkers between electrodes and bioreceptors) and the results (blue data points) demonstrate very low outputs from the sensor (-0.5124±0.2101 %/min, -0.7529±0.1813 %/min, -0.7451±0.3147 %/min, -0.8126±0.4214 %/min for 0.1525 ng/mL, 1.525 ng/mL, 15.25 ng/mL and 152.5 ng/mL influenza A virus in 0.1×PBST

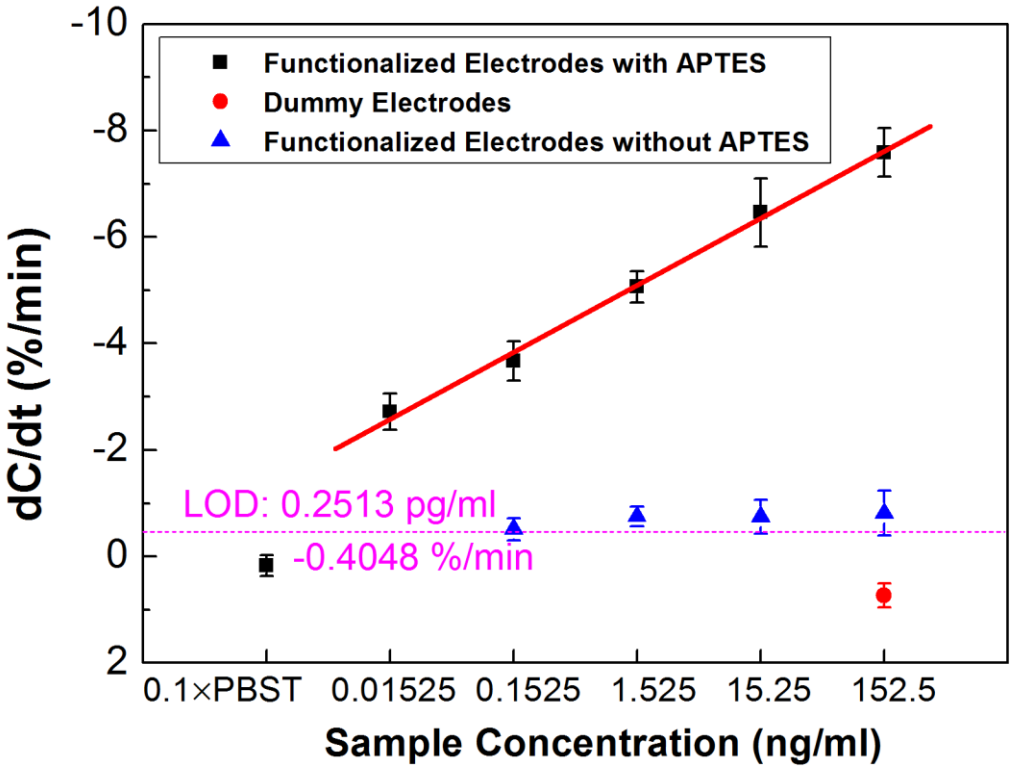

Figure 10 Dose response of influenza A samples as a function of concentration. Tests conducted on electrodes modified with APTES chemical linker (black) yields a linear correlation between sensor output and sample concentrations with an LOD of 0.2513 pg/mL. Tests conducted on electrodes treated with passive functionalization method (blue) demonstrates very small responses.

respectively). In contrast, the sensor's responses are significantly improved by modifying electrodes with APTES before bioreceptors immobilization. Shown as the red data points in Figure 10, the averaged responses of dC/dt are -2.72±0.34 %/min for 15.25 pg/mL virus sample, -3.67±0.37 %/min for 152.5 pg/mL, -5.06±0.29 %/min for 1.525 ng/mL, -6.46±0.64 %/min for 15.25 ng/mL and -7.59±0.46 %/min for 15.25 ng/mL. Reponses of control tests and dummy electrodes are 0.18±0.19 %/min and 0.73±0.23 %/min respectively, which can be easily differentiated from the responses of functionalized electrodes. The dose response can be fitted by Equation 4.1 with a correlation coefficient (R^2) of 0.994.

$$\frac{dC}{dt}(\%/\text{min}) = -1.236 \cdot \lg(x\ (\text{ng/mL})) - 4.855 \qquad (4.1)$$

where *x* is sample concentration in ng/mL.

LOD is defined as three times the standard deviations (0.5816 %/min) from the background response, which is 0.1×PBS-T (0.1769 %/min). The LOD, also the threshold value for differentiating the positive samples from the negative, is calculated to be -0.4048 %/min which corresponds to 0.2513 pg/mL influenza A virus.

5.2 Immobilization buffers

5.2.1 Reagents and samples

5.2.1.1 Zika RNA Washing buffer and blocking reagent

0.5×SSC buffer is prepared by 1:40 dilution of AccuGENE™ 20×SSC Buffer (Lonza, Rockland, ME USA) in ultrapure water. Blocking solution is 1.0 mM 6-mercaptohexanol (Sigma-Aldrich, St. Louis, MO) prepared in ultrapure water. A 5'-thiol-

modified oligo probes, 5'-TTTCGCTCTATTCTCATCAGTTTCATGTCCTGTGTC-3', is synthesized by Fisher Thermo, which is then suspended in DNase/RNase free water to reach a concentration of 100 μM. The probe has a 100% match with Zika virus American Strain with a target region of 1373-1408. It has 26 out of 36 nucleotides matches Zika Uganda strain (targeting Uganda region 1433-1462). DNA probes are diluted to 20 μM in 0.05×PBS.

5.2.1.2 Human herpes virus-1 dsDNA

Testing buffer is based on 20× saline-sodium citrate (SSC) buffer and then diluted to make 2×, 1× and 0.5×SSC in ultrapure water. 5' thiol-modified human herpesvirus 1 probe (HSV-1, 5'- CAAGGCTCACGTGCGAGAGAGCCTCCTC -3')[74] is designed to specifically target UL30 gene of HSV-1, which is then prepared in DNAse/RNAse free water at a concentration of 20 μM. Genomic dsDNAs of Human herpesvirus 1 (HSV-1, Strain McIntyre, ATCC® VR-539D, ATCC, Manassas, VA) and Human herpesvirus 2 (HSV-2, Strain G, ATCC® VR-734, ATCC, Manassas, VA) are prepared in ultrapure water at concentration of 36 μg/mL and 1.3 μg/mL respectively, as stock sample solution.

5.2.2 Sensor performance with various immobilization buffers

Various immobilization buffers (buffers that probe are diluted in for electrodes functionalization) and testing buffers (buffers that target nucleic acid are diluted in for detection) can lead to various sensor performances[75]. Therefore, multiple tests of Zika virus RNA and HSV-1 DNA detections are conducted to define the roles these buffers play in detections. In Figure 11, tests of 18.76×10^3 copies/μL Zika virus RNA sample are conducted on chips with probes prepared in different buffers which would affect the

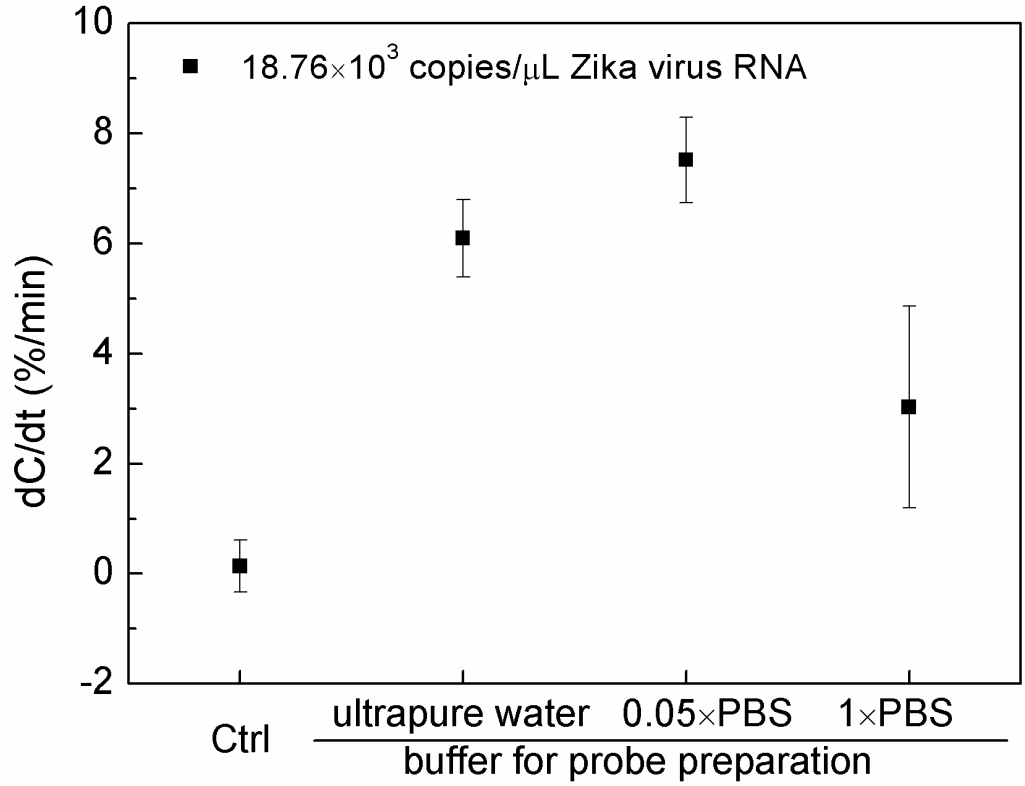

Figure 11 Tests of 18.76×10^3 copies/μL Zika virus RNA sample are conducted on chips incubated with probes prepared in ultrapure water, 0.05×PBS and 1×PBS. Probes in 0.05×PBS is considered to be the optimal due to its high response.

electrodes surface functionalization. Ions in the buffer screen the electrical charges of nuclei acids and allow for higher coverage of electrode surface during immobilization. However, too much ions will cause nuclei acids to coil and lose the ability to bind with other molecules. Buffers of various ionic strengths, including ultrapure water, 0.05×PBS and 1×PBS, is used to functionalized the sensors, and the resultant sensors yield responses of 6.09±0.70 %/min, 7.52±0.78 %/min and 3.02±1.83 %/min, respectively. Clearly, probe in 0.05×PBS leads to the highest response and therefore is used as the optimal immobilization buffer in subsequent experiments.

Further, dose responses of HSV-1 DNA probe in water and 0.05×PBS are obtained and demonstrated in Figure 12. With HSV-1 DNA sample diluted in 0.5×SSC, utilizing 0.05×PBS as buffer for probe incubation (black) gives sensor better performance than ultrapure water (blue). This is because, compared to ultrapure water, 0.05×PBS contains more ions and is able to screen the electrical charges of nuclei acids. It can facilitate probe's immobilization on the surface by allowing for higher coverage of electrodes surface during immobilization.

5.3 Testing buffers

Next, for the testing buffers, similarly, Zika virus RNA and HSV-1 DNA are also utilized for testing. Three concentrations of Zika virus RNA from 187.6 copies/μL (1.0 pg/mL) to 18,760 copies/μL (100 pg/mL) are tested in triplicate with a new functionalized sensor each time. Three concentrations are spiked in 0.5×SSC and 1×SSC solution respectively and tested three times using prepared sensors. Their $d|C|/dt$ responses and standard deviations are shown in Figure 13. The three samples are clearly differentiable

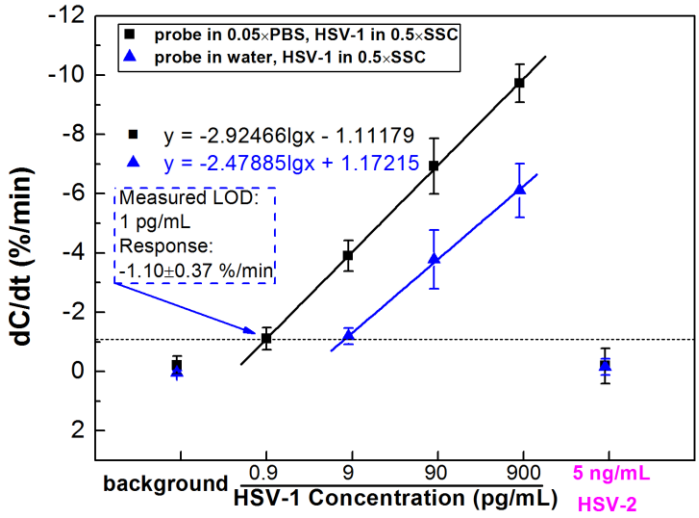

Figure 12 Evaluation of sensor's performances when probe is prepared in 0.05×PBS and ultrapure water. Probe prepared in 0.05×PBS and DNA samples in 0.5×SSC (black) is the optimal immobilization buffer with an LOD of 0.986 pg/mL (6.38 copies/µL or 0.0106 fM).

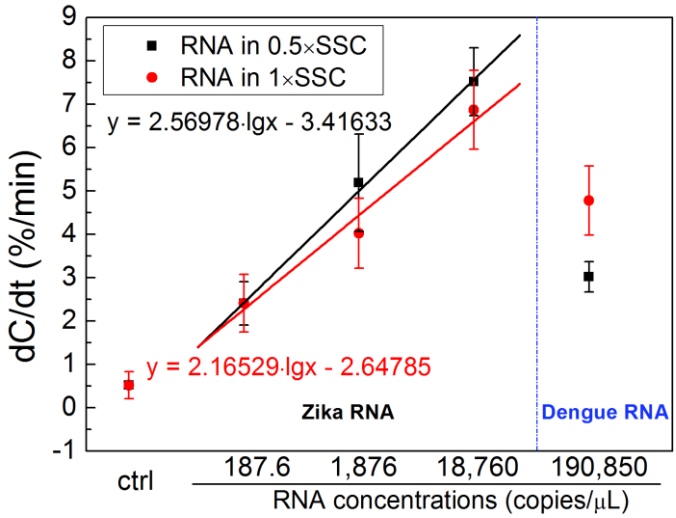

Figure 13 Dose response of Zika RNA spiked in 0.5×SSC and 1×SSC for testing buffer evalution. 0.5×SSC is considered to be the optimal testing buffer and $d|C|/dt$ is 2.40±0.50 %/min for 187.6 copies/µL (1 pg/mL), 5.19±1.12 %/min for 1,876 copies/µL (10 pg/mL) and 7.52±0.78 %/min for 18,760 copies/µL (100 pg/mL), showing a clear logarithmic dependence on Zika virus RNA. Its LOD in 0.5×SSC is yielded to be 0.986 pg/mL (78.825 copies/µL) with a response of 1.458 %/min.

from the background, and their response has a logarithm dependence on concentrations. However, by comparing the slopes of these two curves, target RNA prepared in 0.5× SSC reveals it superiority to the target in 1×SSC. For tests with Zika virus RNA in 0.5× SSC as testing buffer, $d|C|/dt$ is 2.40±0.50 %/min for 187.6 copies/μL (1.0 pg/mL), 5.19±1.12 %/min for 1,876 copies/μL (10 pg/mL) and 7.52±0.78 %/min for 18,760 copies/μL (100 pg/mL). The dependence of $d|C|/dt$ on Zika virus RNA concentration can be approximated fitted as $y = 2.56978 \cdot \lg x - 3.41633$, where x is the Zika virus RNA concentration in copies/μL and y is the capacitance change rate, $d|C|/dt$, in %/min. The LOD is 78.825 copies/μL, or 0.4222 pg/mL, which is defined as 3 standard deviations from the response of background control (0.53±0.31 %/min). The corresponding cut-off $d|C|/dt$ is calculated to be 1.458 %/min.

In a separate experiment, Dengue virus type 2 RNA (New Guinea strain) of 1 ng/ml (190,850 copies/μL) is suspended in both 0.5×SSC and 1×SSC and tested as interference, yielding responses of 3.02±0.35 %/min and 4.78±0.80 %/min respectively. So, given the performances on sensitivity and specificity, 0.5×SSC is used as the optimal testing buffer for Zika virus RNA sample dilution.

As for testing HSV-1 DNA in different testing buffers, as shown in Figure 14, either with 0.05×PBS or ultrapure water for electrodes' functionalization, DNA samples diluted in 0.5×SSC always show higher responses than those in 2× SSC or 1× SSC. It is easy to conclude that buffer used for DNA sample dilution with a relatively low conductivity yields high responses. This is because that relatively low fluid conductivity can result in strong

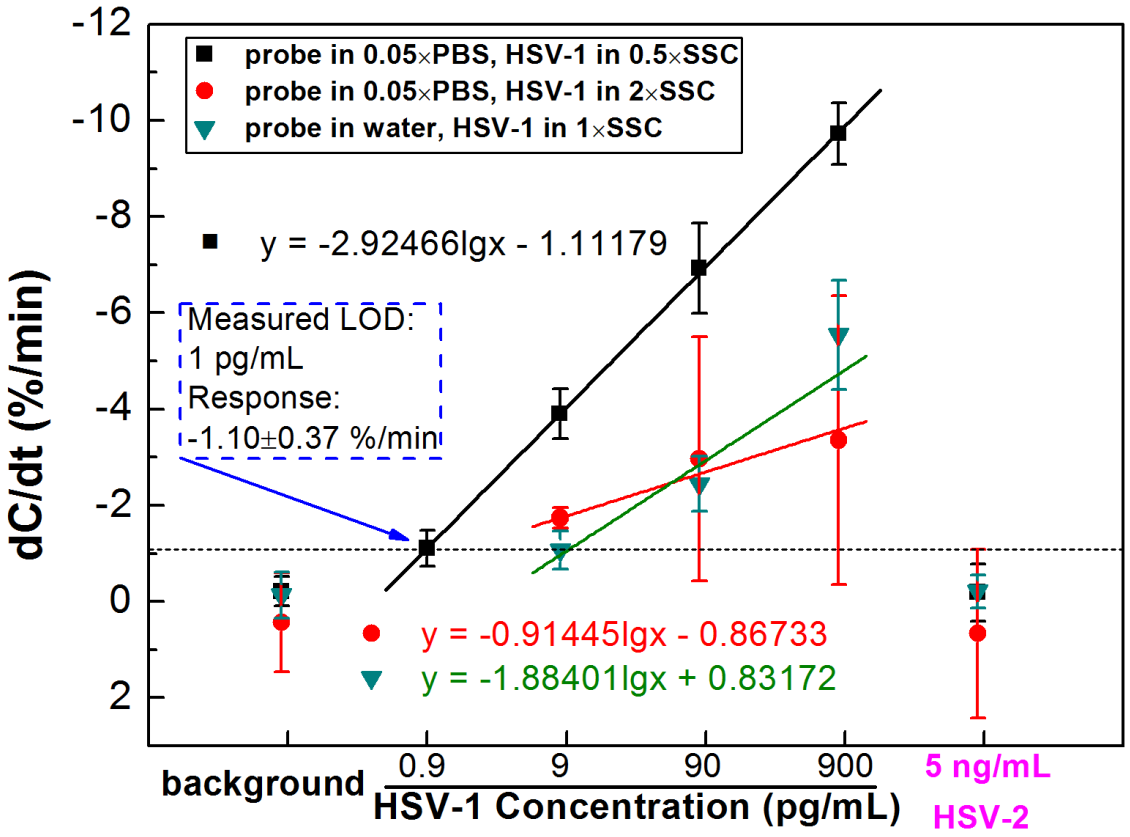

Figure 14 Evaluation of sensor's performances when HSV-1 virus DNA is prepared in 0.5×, 1× and 2×SSC. Probe prepared in 0.05×PBS and DNA samples in 0.5×SSC (black) is the optimal immobilization buffer with an LOD of 0.986 pg/mL (6.38 copies/μL or 0.0106 fM).

DEP effect. In Equation 3.1, lower fluid conductivity gives greater Clausius–Mossotti factor value. Thus, bioparticles in low fluid conductivity will have high DEP velocity.

Based on the given results in Figure 14, HSV-1 probe in 0.05×PBS and HSV-1 DNA (target), HSV-2 (interference) in 0.5×SSC are considered to be optimal with responses of -3.90±0.52 %/min (9 pg/mL), -6.92±0.94 %/min (90 pg/mL) and -9.72±0.63 %/min (900 pg/mL). The sensor's LOD is defined as 3 standard deviations from the response of the background control (-0.22±0.30 %/min), so the cut-off $d|C|/dt$ is calculated to be -1.12 %/min, which corresponds to a HSV-1 DNA concentration of 0.986 pg/mL (6.38 copies/μL or 0.0106 fM). Tests of interference (HSV-2 DNA) also demonstrate a good specificity with a low response of -0.19±0.60 %/min at a concentration (5 ng/mL) 550 times higher than that of HSV-1.

5.4 Applied AC signal frequency and voltage

To elucidate the effects of ACEK mechanisms on detection, the first set of experiments is to find out the effect of AC frequency on the sensor response. Based on Equation 3.1, DEP effects are frequency-dependent. AC signals of various frequencies at 10 mV are used to measure the capacitance changes from influenza A virus samples at a concentration of 1.525 ng/mL. The measured capacitance change rates are given in Figure 15(a). The response shows a bell-shape dependence on AC frequency, with its optimal frequency between 50 kHz and 100 kHz, which indicates that the DEP is the dominant enrichment mechanism. Consequently, AC signal at 100 kHz is considered as the optimized frequency.

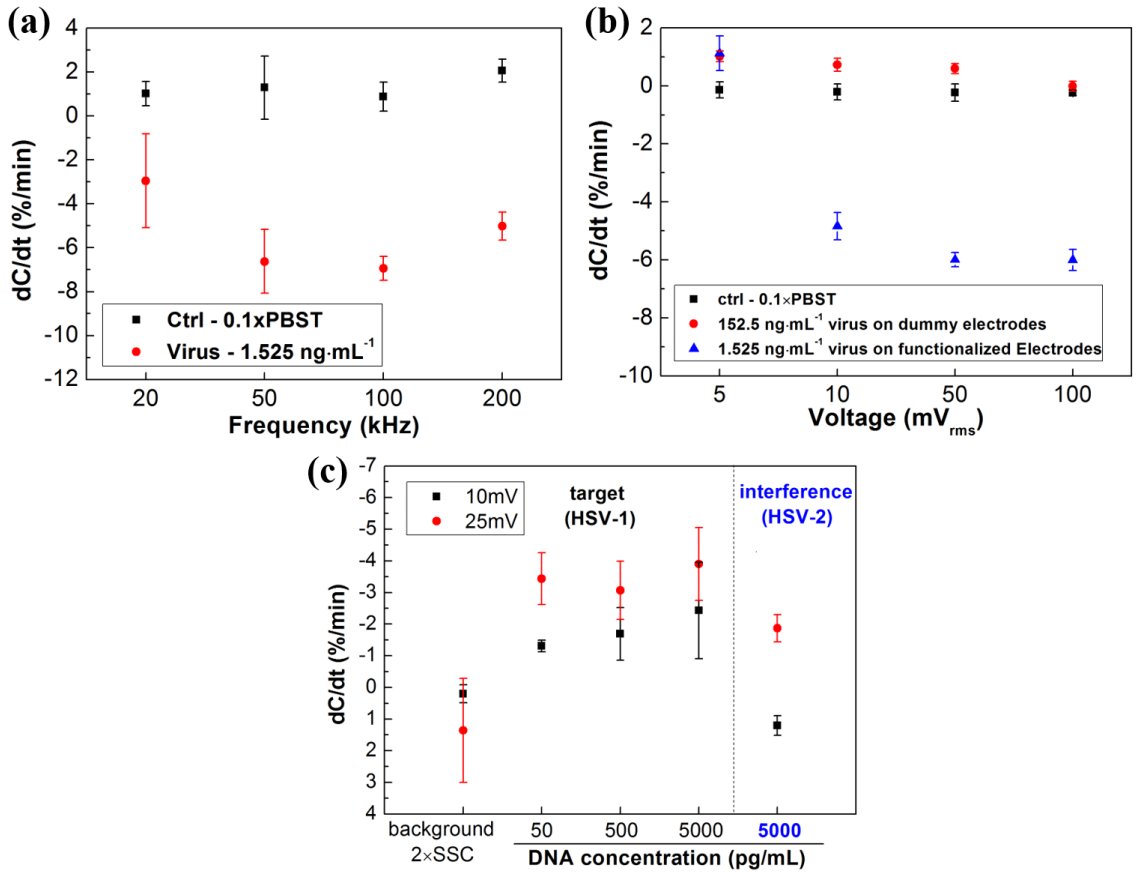

Figure 15 Responses of 0.1×PBS-T, 1.52 ng/mL influenza A virus on functionalized electrodes, and 152.5 ng/mL influenza A virus sample on dummy electrodes (a) when using 10 mV AC signal with its frequency varied from 20 kHz to 200 kHz and (b)when using 100 kHz AC signal with its voltage varied from 5 mV to 100 mV. (c) Responses of 50, 500 and 5000 pg/mL HSV-1 virus DNA and 5000 pg/mL HSV-2 virus DNA.

Next, AC voltages varying from 5 mV to 100 V are used to measure 1.52 ng/mL influenza A virus sample on functionalized electrodes. The background blank buffer, which is 0.1×PBS-T, is also tested on the functionalized electrodes from 5 mV to 100 V as control. Negative control experiments with 152.5 ng/mL influenza A virus sample are measured under the same voltage conditions on dummy electrodes (electrodes without antibody). Experiments with each voltage are repeated three times.

As shown in Figure 15(b), responses of the 0.1×PBS-T control samples on functionalized electrodes and 152.5 ng/mL influenza A virus sample on dummy electrodes remain quite small through the voltage range of 5-100 mV, with a limited response ranged from -0.14 to -0.24 %/min and 1.02 to -0.01 %/min. For tests on functionalized electrodes, due to DEP effect, the capacitive response decreases as the voltage increases from 5 to 100 mV, indicating that more binding takes place with higher AC voltage. When the voltage level is above 10 mV, the increase of sensor's response becomes limited due to saturation of binding sites on the sensor. Therefore, 10 mV is chosen as the measuring voltage. At this voltage, DEP effect will be weak for particles smaller than virus such as protein to cause appreciable capacitance change[69], therefore improved the sensor specificity in complex matrix. This can also be justified by the tests of HSV-1 virus DNA conducted under 10 mV and 25 mV in Figure 15(c). While the sensor yields higher outputs at 25 mV, the sensor also shows non-negligible responses (-1.87±0.43 %/min) to 5 ng/mL HSV-2 DNA. In contrast, the response of 5 ng/mL HSV-2 DNA is 1.21±0.31 %/min at 10 mV, which is considered to a negative response as it cannot be differentiated from that of the background. A good sensor requires the sensor to have large responses to target molecules

with little to none responses non-targets. Test results of HSV-1 and HSV-2 indicate that using AC signal at 10 mV can achieve good specificity with only slight compromise on response (dC/dt values). Therefore, 10 mV is also considered to be superior to 25 mV in detection of HSV-1 virus DNA.

5.5 Summary of the sensing platform's performances

For the four different pathogen targets in standard matrices studied previously, Table 2 summarizes their assay time, LODs, and matrices in which the LODs are obtained. The performances of the biosensing platform in this work are significantly improved. It can detect specific targets within 30 seconds, with quite low LODs in pg/mL or fg/mL levels. The sensor also demonstrates good specificity against other interferences, which make it has a great potential to be used for testing in complex sample matrices.

Table 2 Summary of the sensing platform's performance on detecting various pathogens.

Target	Matrix	LOD	Assay time
influenza A virus	0.1×PBS-T	0.25 pg/mL	30 seconds
protein IgG/pseudorabies	0.1×PBS	4.5 fg/mL	30 seconds
DNA/Human herpesvirus 1	0.5×SSC	0.986 pg/mL	30 seconds
RNA/Zika	0.5×SSC	1 pg/mL	30 seconds

CHAPTER 6

VARIOUS APPROACHES FOR PATHOGENS DETECTION IN COMPLEX MATRICES

6.1 Influenza A virus

Clinical nasal swab Influenza A virus sample with nasal swab is immersed in M4RT[76] are provide by a company and a serial dilution up to 1:10000 is applied using 0.1×PBST. It is common practice to dilute clinical samples in standard buffer. Due to the complexity of clinical samples, highly diluted samples can reduce non-specific binding, which improve the selectivity of the sensor. With more dilution of clinical samples, chances of false positive results can be reduced. However, sensor's sensitivity will also suffer since the concentration of target particles is reduced at the same time. The optimization dilution factor helps to decide which dilution can be used for the bind tests of unknown swab samples in the next step. In addition, unlike the spiked samples in previous sections, clinical swab samples are in M4RT instead of 0.1×PBS-T. M4RT is a liquid medium commonly used in the transport of clinical specimens to the laboratory for qualitative microbiological procedures for viral and chlamydial agents. M4RT with no dilution can cause a decrease in capacitance (-0.48±0.035 %/min), but for M4RT with 1:1,000 dilution or more in 0.1×PBS-T its effect can be neglected (0.46±0.45 %/min at 1:1000 dilution). So dilution factors higher than 1:1000 are studied in Figure 16. To find out the optimal dilution factor to test, two clinical nasal swab samples (one positive and one negative) at various dilution factors from 1:100,000 to 1:1,000. Each sample is tested in triplicates, and each chip is

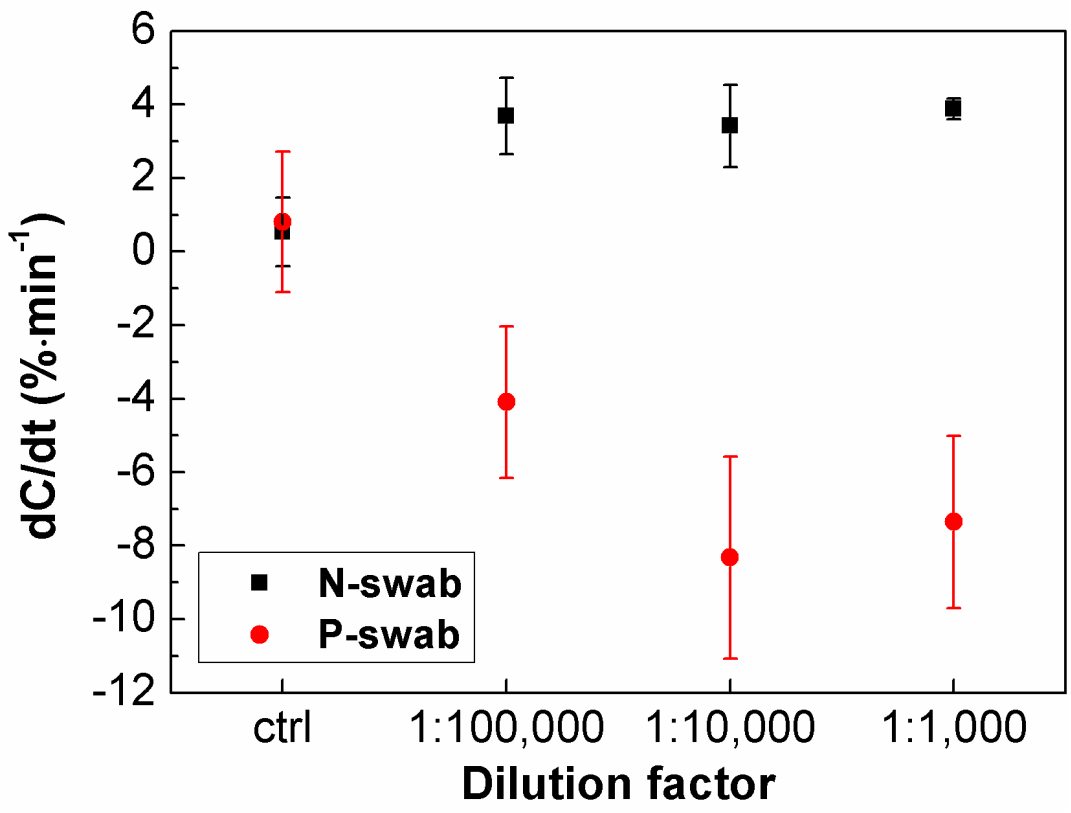

Figure 16 Responses of clinical negative and positive swab samples of dilution factor of 1:100,000, 1:10,000 and 1:1,000.

tested with three dilutions in the sequence of 1:100,000, 1:10,000 and 1:1,000. Based on the sensor's readout in Figure 16, response reaches the highest at 1:10,000 dilution of positive sample. The 1:1000 dilution did not yield a larger response due to the saturation of the limited available binding sites on the electrode's surface. Nevertheless, 1:100,000 dilution is adopted instead of 1:10,000 since the response of sample at 1:100,000 dilution (-4.09±2.06 %/min) is located around the median of the dose response line shown in Figure 10. So 1:100,000 dilution is chosen in order to acquire a larger dynamic range in sensor response, desirable for clinical swab samples measurement in blind tests.

Blind tests for a panel of 20 nasal swab samples (10 positive, 10 negative) are conducted. All samples are 1:100,000 diluted with 0.1× PBS-T. The threshold value is set at -0.40 %/min, which is also the LOD from previous tests with spiked samples, meaning that samples with a response more negative than -0.40 %/min will be considered as positive samples and others negative. As shown in Figure 17(a), 9 out of 10 positive and 7 out of 10 negative samples are correctly identified by ACEK capacitive sensors. A negative sample with influenza B virus is also correctly identified. All these samples are verified by RT-qPCR, yielding a sensitivity of 90% and specificity of 70% for the panel. Figure 17(b) shows a positive correlation between the capacitance change rate and PCR cycles number. Weak positive samples are chosen for this set of experiments. Among all the detected positive samples, only the sample with the highest response can be detected by a commercial RIDT, which corresponds to 22 PCR cycles. ACEK capacitive sensor can detect virus level corresponding to 35 PCR cycles. There is a false negative corresponding to 29 PCR cycles. This is possibly due to error during dilution or the binding site on the

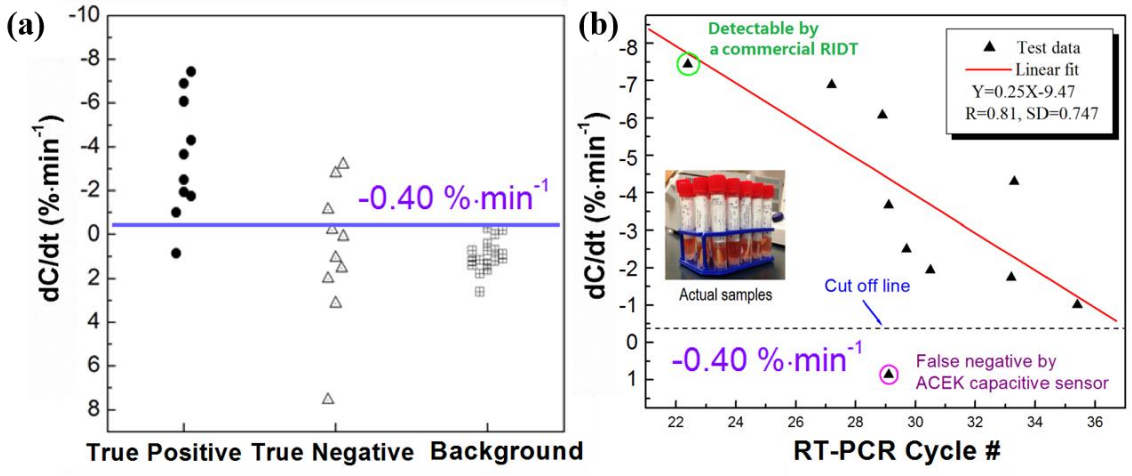

Figure 17 Comparison of results from ACEK capacitive sensors and those from commercial tests for a blind panel test of influenza virus A from nasal swabs. (a) Responses of all tested samples differentiated by the -0.40 %·min^{-1} cut-off line (blue) and (b) correlation between PCR cycles and responses of samples determined as positive by ACEK capacitive sensor in blind tests. The strongest positive sample is the limit of a commercial rapid influenza test.

virus not being exposed.

6.2 Protein (antibody to pseudorabies virus)

Serum spiked goat anti-bovine IgG antibody samples are tested to demonstrate the sensor's performance in complex matrix. HyClone™ Fetal Bovine Serum (U.S.), Standard (FBS) is purchased from Fisher Scientific, Waltham, MA. It is then 1:10 and 1:100 diluted in 0.1×PBS-T to obtain 1:10 and 1:100 FBS solution respectively for preparing of goat anti-bovine IgG serum spiked samples. In order to gauge the effect of FBS matrix at various frequency, 1:10 and 1:100 FBS are tested under the applied AC signal ranges from 20 kHz to 200 kHz in Figure 18(a). The sensor response is found to decrease with increasing frequency for both 1:10 and 1:100 FBS. However, 1:100 FBS demonstrate essentially lower responses than 1:10 FBS. Therefore, dose response of protein in serum matrix is studied by spiking goat anti-bovine IgG into 1:100 FBS at concentrations of 10, 100 and 1000 fg/mL in Figure 18(b).

Next, pseudorabies virus clinical samples, three positive and three negative, are tested. The swab samples are diluted 1:10,000 v/v% in 0.1×PBS-T solution, which. contains 0.05 v/v% Tween 20 (Fisher Scientific, Pittsburgh, PA), Positive samples can be clearly differentiated from negative samples in Figure 19.

6.3 Nucleic acids RNA and DNA

6.3.1 Reagents

Human blood samples are collected from pregnant women who entered labor and

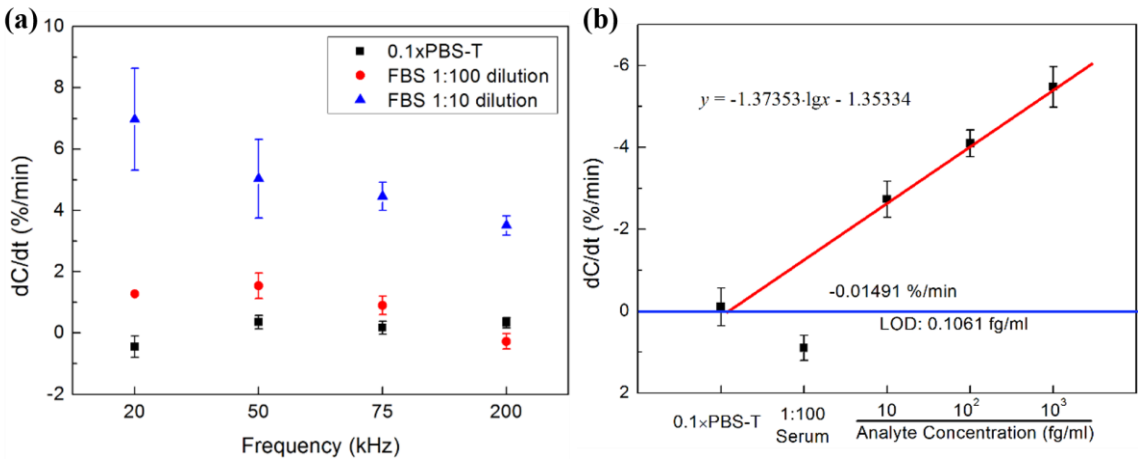

Figure 18 (a) Responses of FBS in different dilution rates. (b) Dose response of protein IgG in 1% serum matrix.

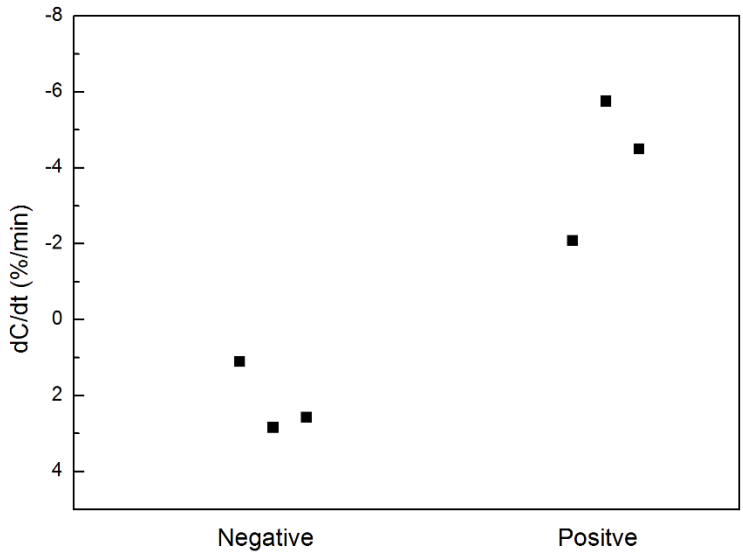

Figure 19 Tests of pseudorabies virus clinical samples. Positive and negative samples can be clearly differenced.

delivery at the University of Tennessee Medical Center, Knoxville. All samples andclinical information are collected under clinical research protocols approved by the University of Tennessee Institutional Review Boards. These human blood samples are centrifuged at 2,000 rpm for 15 minutes and sera are pooled. After being diluted 1:100 in 0.1×PBS, the obtained 1% serum sample is then 1:1 mixed with lysing solution, which contains 1 mM Tris (pH 8.0), 2 mM EDTA, 1% SDS and 2 mg/mL Proteinase K (Fisher BioReagents, Pittsburgh, PA).

Quantitative genomic RNA from Zika virus is purchased from ATCC (ATCC® VR-1838DQ, ATCC, Manassas, VA) and diluted in serum/lysing solution to 0.1876×10^3 copies/μL (1.0 pg/mL), 1.876×10^3 copies/μL (10 pg/mL), 18.76×10^3 copies/μL (100 pg/mL), 187.6×10^3 copies/μL (1 ng/mL) and 1876×10^3 copies/μL (10 ng/mL), respectively. Quantitative genomic DNA from human herpesvirus 1 (HSV-1) (ATCC® VR-539DQ™, ATCC Manassas, VA) is diluted in serum/lysing solution for a concentration of 6.585×10^3 copies/μL (1 ng/mL). Dengue virus type 2 (New Guinea strain) is diluted in serum/lysing solution to 19,095 copies/μL (0.1 ng/mL) respectively. Influenza A virus (gift from a company) is suspended in serum/lysing solution to 1.525 ng/mL

6.3.1 Zika virus RNA

Five concentrations of Zika virus RNA are spiked in 1:1 mixture of 1% serum and lysing solution, and tested using functionalized sensors. Each concentration is tested in triplicates with a new chip each time. Like the samples spiked in 0.5×SSC, five Zika virus RNA spiked serum samples are clearly differentiated from each other and the background. As shown in Figure 20, $d|C|/dt$ is 2.04±0.22 %/min for 0.1876×10^3 copies/μL (1.0 pg/mL),

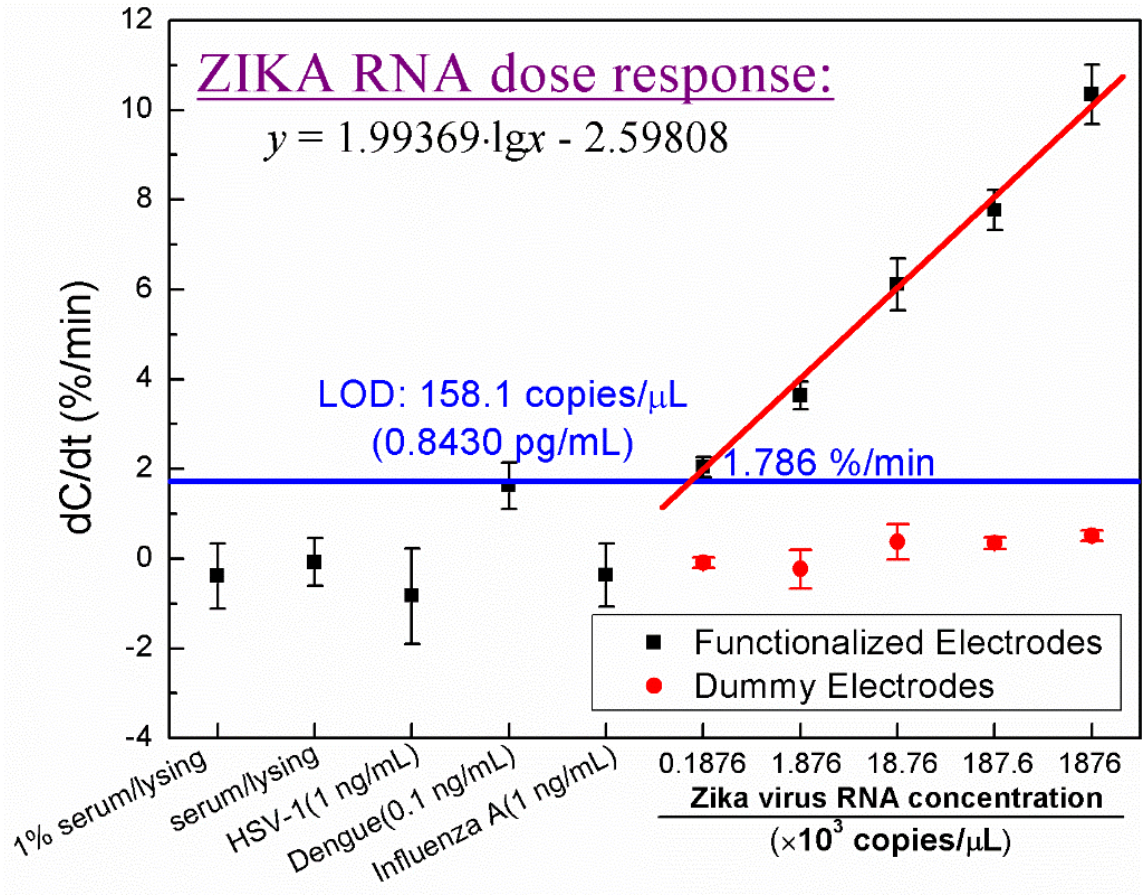

Figure 20 Responses of non-specific nuclei acid (HSV-1 and dengue) and virus (influenza A), and dose response of Zika virus RNA spiked in serum/lysing solution.

gradually increasing to 7.77±0.45 %/min for 1,876×10^3 copies/μL (10 ng/mL) RNA. *d|C|/dt* shows a clear logarithmic dependence on Zika virus RNA concentration over at least four orders of magnitude from 1.0 pg/mL to 10 ng/mL. The dependence of *d|C|/dt* on Zika virus RNA concentration can be approximated as y=1.99369·lg$x$-2.59808, where x is Zika virus RNA concentration in copies/μL and y is capacitance change rate, *d|C|/dt*, in %/min. The fitted line had a correlation coefficient of 0.97, and is used as the sensor standard curve. The LOD is defined as 3 standard deviations from the response of the background control. Because the background produced a response of -0.39±0.72 %/min, the cut-off *d|C|/dt* is calculated to be 1.786 %/min, which corresponded to a Zika virus RNA concentration of 158.1 copies/μL, or 0.846 pg/mL. The LOD of Zika virus RNA in serum is slightly higher than that of RNA in SSC (78.8 copies/μL), which is expected due to more interference molecules in serum. To exclude possible artifacts as causes of sensor response, control tests are conducted by applying Zika virus RNA samples of the same concentrations on dummy electrodes (without functionalization, and only blocked with 1.0 mM 6-mercaptohexanol in ultrapure water). As shown in Figure 20, the responses from the dummy electrodes are negligible, at -0.092±0.12 %/min, -0.23±0.43 %/min, 0.38±0.39 %/min, 0.35±0.13 %/min and 0.51±0.12 %/min respectively, which are very similar to the response of fluid background. This indicates that the responses from active sensors are indeed caused by the hybridization between the probe and the target RNA.

In Figure 21, with the same lysing solution containing 1% serum, sensors functionalized with three different probes are tested and compared. The probe used previously in Chapter 5 is denoted as Probe #0. Probe #1 has a sequence of

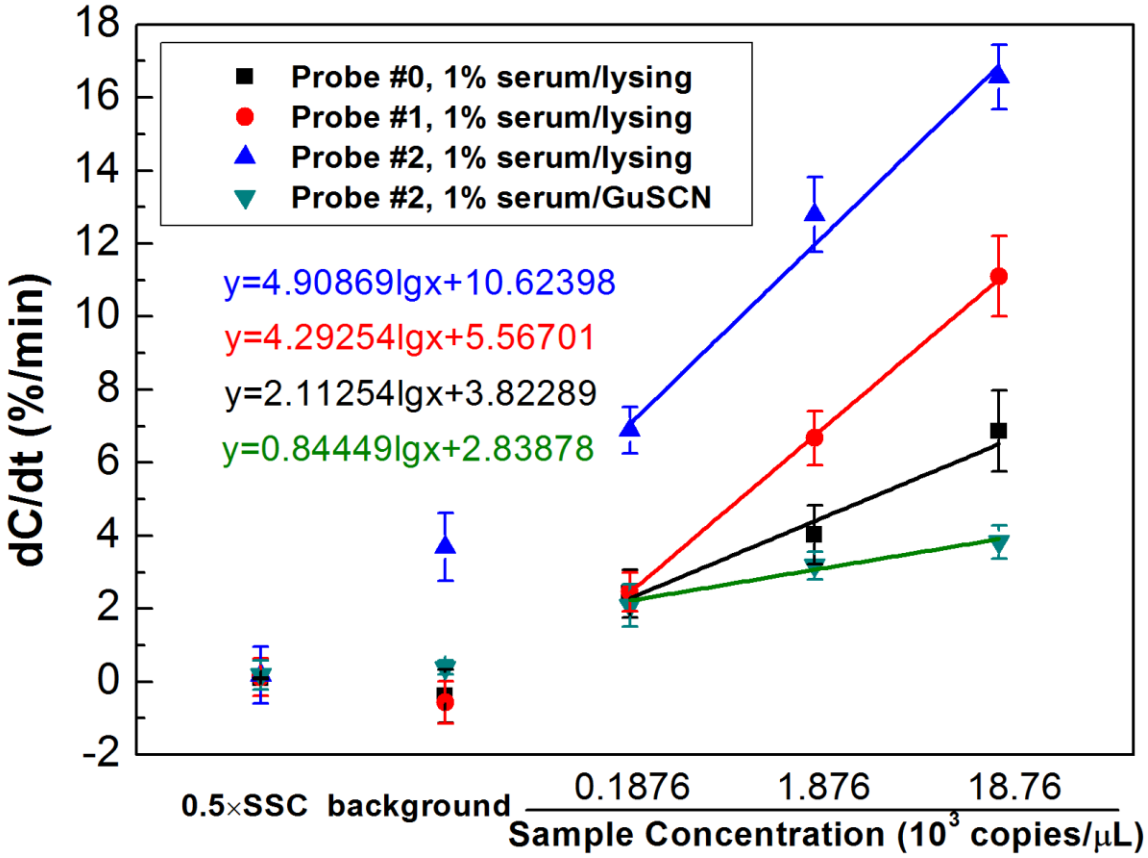

Figure 21 Responses of Zika virus RNA in lysing or GuSCN solution containing 1% serum by various probes.

TCTTCAGCCTCCATGTGTCATTCTTTTCACTTTCAA, and Probe #2 has a sequence of TTTCGCTCTATCTTCGTCAGTTTCATATCCAATCAT. Probe #1 and #2 both have a 100% match with Zika virus Uganda Strain, with target genomic sequence regions of 3116-3081 and 1427-1462 of Zika virus (strain MR 776, GenBank: AY632535.2)[77].

Although responses by sensors functionalized with Probes #1 and #2 show higher sensitivity than those with Probe #0, Probe #2 demonstrates a much higher sensor readouts. By comparing results of target RNA prepared in 1% serum/lysing and 1% serum/GuSCN, it can be concluded that diluting Zika RNA into testing buffer containing GuSCN solution (green) does not make any improvement over that into lysing solution (blue). This might be due to the high conductivity that GuSCN has. At sensor's working frequency of 100 kHz, the equivalent circuit of the sensor electrodes can be simplified as bulk solution resistance R_s in serial with interfacial capacitance C_{int}. The bulk solution resistance is 3.28 kΩ and 84.1 Ω in 1:1 mixture of 1% serum/lysing solution and 1:1 mixture of 1% serum/GuSCN solution respectively. The impedance of interfacial capacitance is calculated to be 564.9 Ω in 1% serum/lysing solution and 39.9 Ω in 1% serum/GuSCN solution. Consequently, 85.32% of the total applied AC signal (~8.53 mV) is applied over the bulk 1% serum/lysing solution and 67.78% (~6.78 mV) over the bulk 1% serum/GuSCN solution. Therefore, with buffer in lower conductivity, more electric field is applied and utilized to induce DEP for bioparticle enrichment.

Next, sensor's specificity is evaluated by using Dengue virus RNA as interference. Probe # 1 and # 2 are used for sensor electrodes functionalization and both Zika virus RNA (target) and Dengue virus RNA (interference) are spiked into 1:1 mixture of serum and

lysing solution. Given 2×SSC solution's aid in RNA target-probe hybridization, 2×SSC is adopted to make 1:1:1 mixture of serum, GuSCN and 2×SSC to improve the performance of testing buffer containing GuSCN solution used in previous assay (green curve in Figure 21). Therefore, Zika and Dengue virus RNA are also spiked into 1:1:1 mixture of serum, GuSCN and 2×SSC to find out the optimal combination of probe and testing buffer which would offer both excellent sensor sensitivity, readouts, as well as specificity. In figure 22(a) and 23(b), for Probe #1, tests of Dengue virus RNA utilizing 1:1:1 mixture of serum, GuSCN and 2×SSC as testing solution demonstrates both lower responses and curve slope, meaning 1:1:1 mixture of serum, GuSCN and 2×SSC as testing solution shows superiority in sensor's specificity. The similar results are also observed in tests with Probe #2 (Figure 22(c) and 22(d)). In addition, by adding 2×SSC, sensor also yields higher response compared with responses from previous GuSCN solution. Thus, if comparisons are made between Figure 22(a)(c) and Figure 22(c)(d), it can be easily concluded that sensor yields the optimal performances on sensitivity and specificity with electrodes functionalized with Probe #2 and target Zika RNA (interference Dengue virus RNA) in 1:1:1 mixture of serum, GuSCN and 2×SSC as testing solution.

In Figure 23, the percentage rate of serum in the optimized testing buffer is adjusted from 33% to 50% (from 1:1:1 mixture to 2:1:1). In order to be able to evaluate the effect this adjustment will have on the sensor's performance, the Zika virus RNA concentration is converted into the equivalent concentration in pure serum.For the adjusted testing buffer of 2:1:1 mixture, sensor indicates a less sensitive dose response with 2.29±0.20 %/min for 0.3752×10^3 copies/μL, 5.23±0.46 %/min for 3.752×10^3 copies/μL and 9.08±1.07 %/min

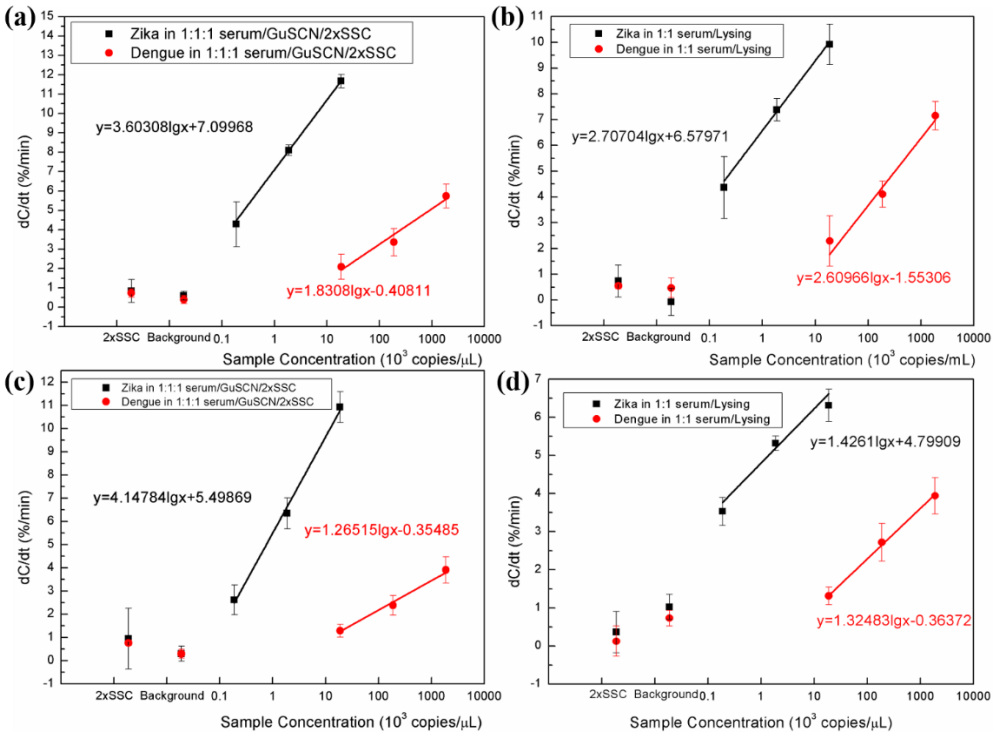

Figure 22 Zika and Dengue virus RNA responses with various probes (Probe #1 and #2) and testing buffer containing pure serum: (a) Probe #1 with 1:1:1 of serum, GuSCN and 2×SSC as testing buffer; (b) Probe #1 with 1:1 of serum and lysing solution as testing buffer; (c) Probe #2 with 1:1:1 of serum, GuSCN and 2×SSC as testing buffer; and (d) Probe #2 with 1:1 of serum and lysing solution as testing buffer.

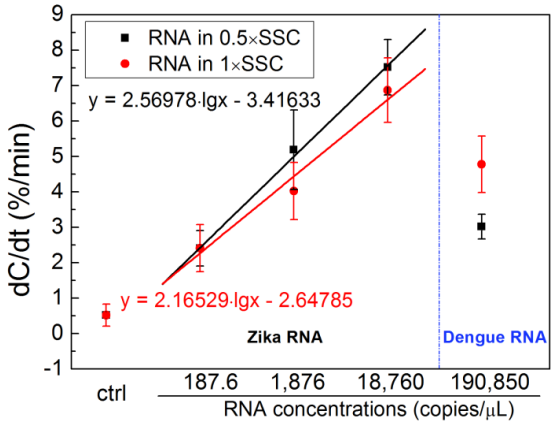

Figure 23 Responses of tests on Probe #2 functionalized electrodes vs. Zika virus RNA concentration converted into pure serum.

for 37.52×10^3 copies/μL.While for 1:1:1 mixture, 0.5628×10^3 copies/μL, 5.628×10^3 copies/μL and 56.28×10^3 copies/μL Zika virus RNA in pure serum have responses of 2.62±0.64 %/min, 6.33±0.67 %/min and 10.92±0.66 %/min respectively.

6.3.3 HSV-1 DNA

In order to avoid the protein sediment in serum when samples are heated to 95 °C for DNA denaturation, DNA serum spiked samples are diluted into lysing solution. Lysing solution can break down peptide bonds, digest proteins in serum and help reduce sediment that may affect DNA hybridization during tests. In Figure 24, 900 pg/mL HSV-1 DNA in undiluted serum is 1:2, 1:2.5, 1:3.3, 1:5, 1:10 and 1:20 diluted into lysing solution respectively before denaturation (actual concentration in serum is 450 pg/mL, 360 pg/mL, 270 pg/mL, 180 pg/mL, 90 pg/mL and 45 pg/mL). For dilution factor ranged from 1:2 to 1:20, sensors' responses are 0.50±0.19 %/min, -1.38±0.55 %/min, -2.46±0.15 %/min, -3.437±0.28 %/min, -5.64±0.59 %/min and -6.34±0.49 %/min with a background response of -0.38±0.20 %/min. It can be concluded that serum spiked samples with more dilution will yield higher $d|C|/dt$ responses. 1:20 and 1:10 in Figure 24 shows the highest yet comparable responses. Therefore, dilution factors of 1:20 and 1:10 are used in the subsequent experiments of HSV-1 DNA spiked serum samples.

Figure 25 demonstrates the logarithmic dependence of HSV-1 DNA concentrations on sensor response ($d|C|/dt$ in %/min). The shown HSV-1 DNA concentrations are concentrations in neat serum, which are 90 pg/mL, 900 pg/mL and 9 ng/mL. Two dilution factors of 1:20 and 1:10 show similar performances in Figure 25. The LOD are calculated

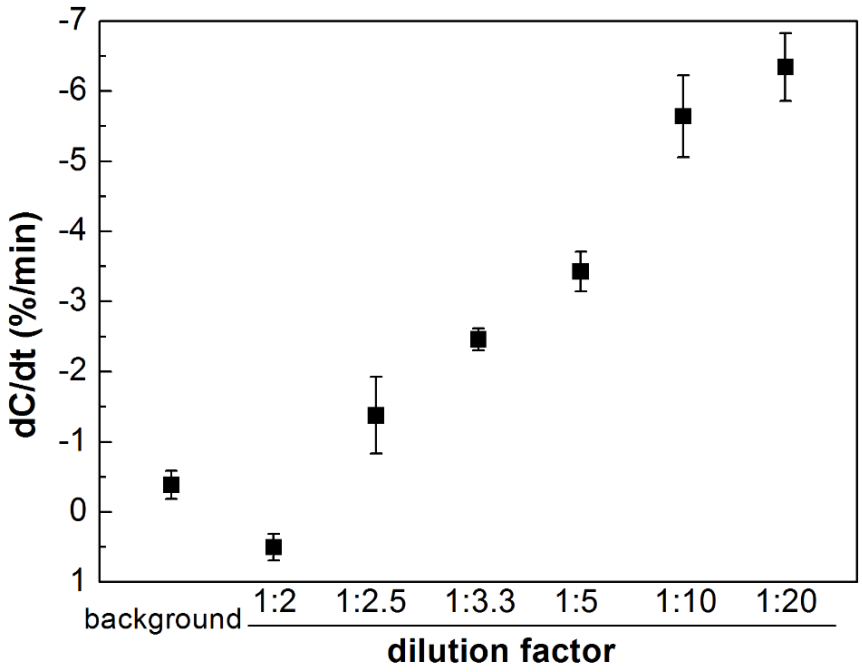

Figure 24 Responses of DNA spiked serum diluted in lysing solution using different dilution factors.

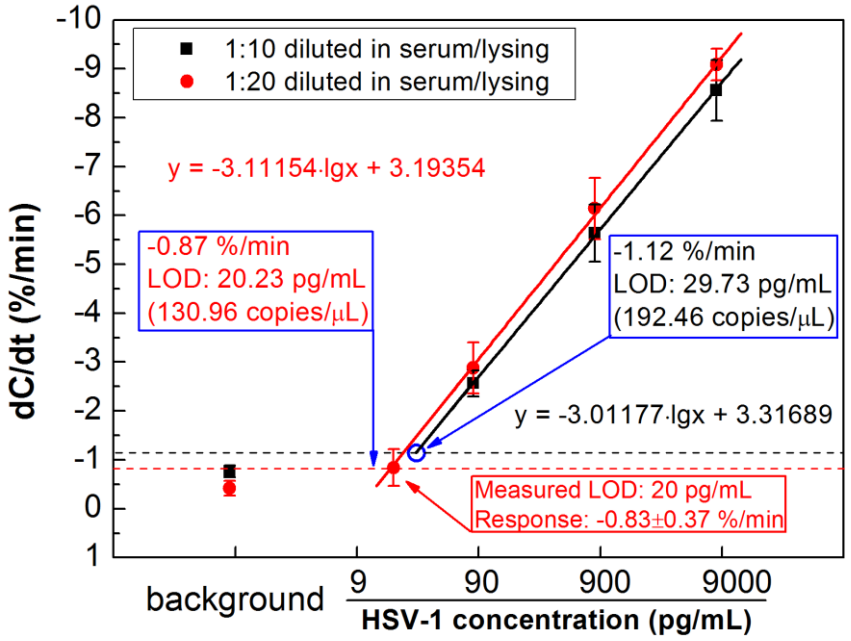

Figure 25 Dose response of HSV-1 DNA serum samples with 1:20 and 1:10 dilution.

to be 19.46 pg/mL (125.98 copies/μL or 0.21 fM) and 29.73 pg/mL (192.46 copies/μL or 0.32 fM) for 1:20 and 1:10 dilution respectively. Since samples with 1:20 dilution show slight advantages on sensitivity, LOD and sensor readouts, it is considered to be the optimal dilution factor for HSV-1 DNA spiked serum sample tests.

CHAPTER 7

EXPANSION TO CHEMICAL DETECTION

Reproduced in part with permission from **Bisphenol A Sensors on Polyimide Fabricated by Laser Direct Writing for Onsite River Water Monitoring at Attomolar Concentration**, Cheng Cheng, Shutong Wang, Jayne Wu, Yongchao Yu, Ruozhou Li, Shigetoshi Eda, Jiangang Chen, Guoying Feng, Benjamin Lawrie, and Anming Hu, *ACS Applied Materials & Interfaces* **2016** *8* (28), 17784-17792, DOI: 10.1021/acsami.6b03743.

In recent years, there is an increasing interest in developing effective tools for bisphenol A (BPA) detection in the environment and food supply. Different from the protein, virus or nucleic acids in size, BPA is small molecule and a different ac electrokinetics mechanism, ac electroosmotic (ACEO) effect, is used for more effective transport of the target analyte in water. In this work, ACEO-based capacitive sensing is used to detect the binding of BPA with aptamer at the electrode surface. In additional, to further reduce the sensor cost and improve the LOD for water monitoring, laser printed electrodes on polyimide are adopted as the sensor in this work.

7.1 Electrodes fabrication

The laser written electrodes used in this work are fabricated by a femtosecond (fs) pulsed laser (Cazadero, Calmar Laser Inc.) and a 532 nm CW laser (Verdi G5, Coherent) via a 20 × microscope objective (NA=0.42) on the flexible Polyimide (PI) sheet (Kapton_HN, 100 μm thickness) (Figure 26(a)). The fs laser generates pulses with 1030

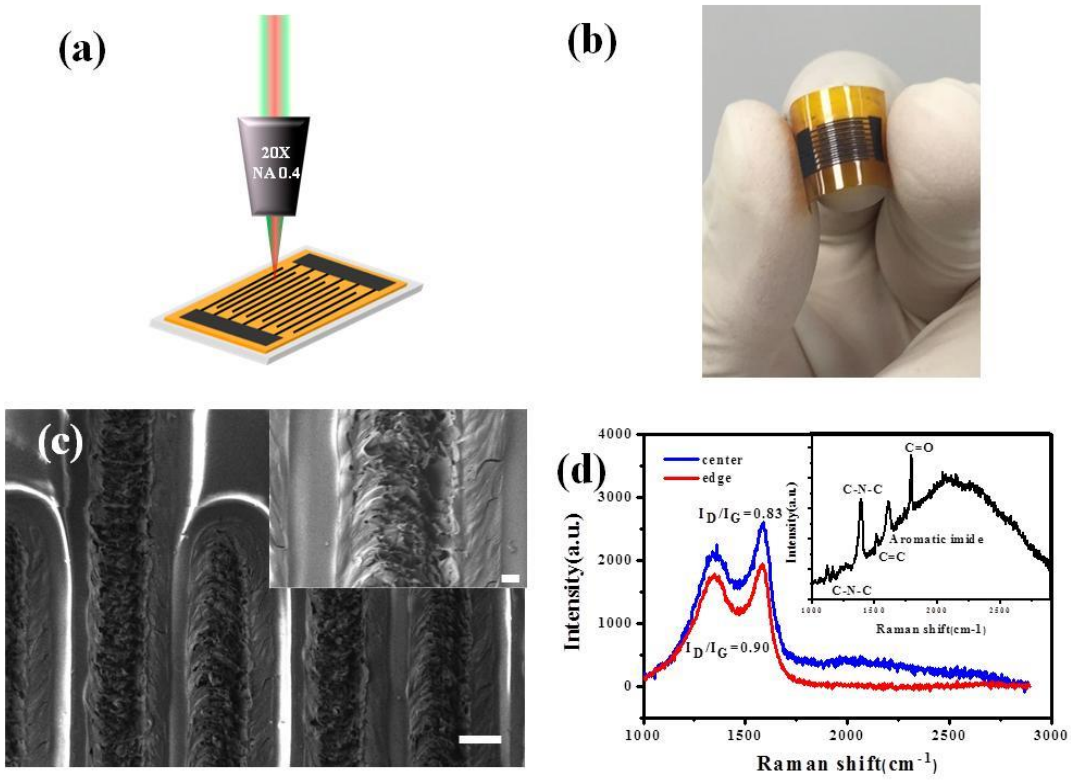

Figure 26 (a) Schematic illustration of the laser direct writing of electrode on a polyimide substrate, (b) Typical photo image of flexible electrodes, (c) SEM images of the porous carbonized structures and (d) Raman spectra of the polyimide regimes with and without laser irradiation.

nm central wavelength, and 400 fs pulse duration at a repetition rate of 120 kHz. The PI films are mounted on an XY-translation stage controlled by a computer. In our case, the fs laser and CW laser power concentrated on the sample surface are 230 mW and 85 mW with a spot size of 3-5 μm, respectively, and a scanning speed of 0.5 mm/s. All irradiation is performed in air environment under normal incidence. The gap distance between adjacent finger electrodes is fixed at 90 μm, and a total of 8 pairs of electrode fingers are written in one sensor (Figure 26(b)). The generation of black lines on the polyimide sheet after the laser scanning confirmed the carbonization of the polymer. Figure 26(c) illustrates the porous flake structures of the irradiated regimes. This porosity is a result of polyimide molecules initially dissociating in the vicinity of focal point of the fs laser as a result of multi-photon absorption[78]–[80]. Raman spectra shown in Figure 26(d) indicates the recorded at three areas under excitation at 532 nm: (1) near the center of the carbonized electrode, (2) about 40 μm away from the center, and (3) at the unexposed PI film.

Prior to irradiation, the PI film is cleaned using ethanol. Finally, the surface morphology is observed using optical microscopy and scanning electronic microscopy (Zeiss Auriga). After surface treatment by plasma cleaner or ozone cleaner, a microchamber is attached to the foil surface for surface functionalization and subsequent sensing.

Appropriate working frequency is also vital in this work and can be found and estimated by the equivalent circuit cell fitting. For example, an optimal frequency at which ACEO flow velocity peaks for a given AC voltage needs to be selected in the BPA

detection. Referring to Equation 3.2, E_t is dependent on the bulk impedance (R_s and C_s) and $\Delta\xi$ is dependent on the interfacial impedance (R_{ct} and C_{int}).

By fitting the measured impedance spectrum with the equivalent circuit model of laser writing electrodes shown in Figure 2, the values for each circuit element in Figure 2 are found as follows, R_{wire} = 450 Ω, C_{int} = 0.7 μF, R_{ct} = 30 kΩ, R_s = 500 Ω and C_s = 6.1 pF. The fitting curves along with the measured impedance data are shown in Figure 27. At low frequency (below 100 kHz), the electrical current between an electrode pair predominately takes the path formed by C_{int} and R_s.

7.2 Reagents and samples

20 μM BPA aptamer in ultrapure water is used for incubation. Analytical BPA samples are prepared as 0.1 fM, 1.0 fM, 10 fM, 100 fM and 1 pM BPA in ultrapure water. Surface water samples are collected from Tennessee River near a waste water treatment plant in Knoxville and are diluted at 1:1,000,000 in ultrapure water prior to testing. No filtering is performed.

7.3 Capacitance change with time during assay

Ultrapure (Mili-Q) water as the background solution is also tested as the control. Each measurement is performed with an AC signal of 300 mV, 1 kHz for 20 seconds. As shown in Figure 28, the negative samples of 10 pM BPS (0.14 %/min) and BPF (0.35 %/min), and the control sample (-0.66 %/min) exhibited virtually no measurable shift in capacitance, while the positive samples containing trace BPA in water, gave a capacitance change of -19.39 %/min, -21.40 %/min, -29.65 %/min, -38.20 %/min and -44.10 %/min at 1 fM, 10 fM, 100 fM and 1 pM respectively.

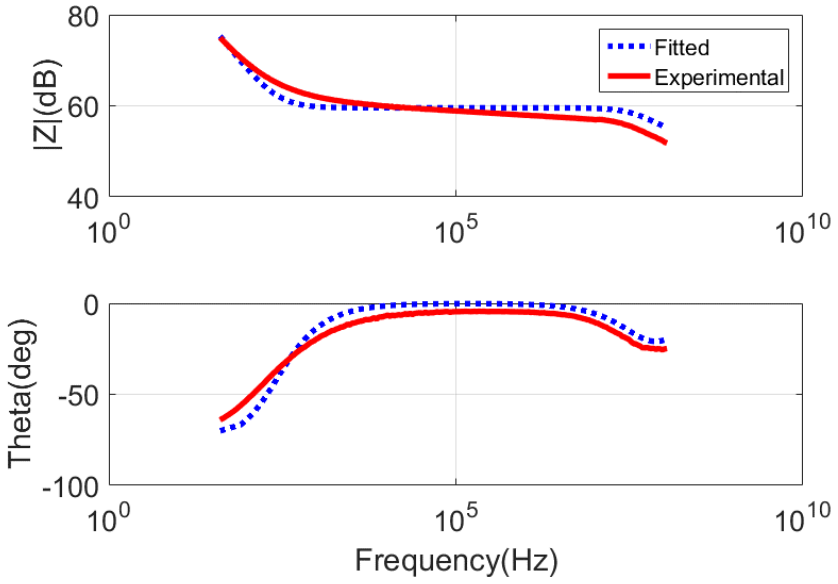

Figure 27 The measured impedance spectra (solid line) of the electrode cell and its equivalent circuit fitting (dotted line).

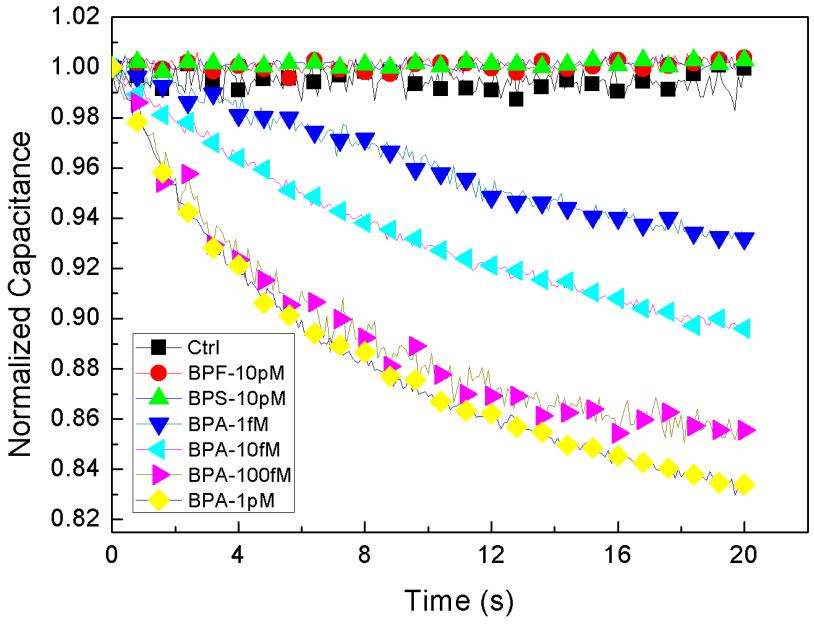

Figure 28 Normalized capacitance changes of control, BPA, BPS and BPF samples with time.

7.4 Working condition optimization

Based on Equation 3.2, ACEO flow velocity is strongly dependent on the voltage and frequency. Therefore, AC voltage level and frequency need to be optimized to fully take advantage of ACEO effect. Figure 29 shows the results when optimizing AC voltage level and frequency. All the tests are performed with 1fM BPA in ultrapure (Mili-Q) water. First the sensor responses are measured with AC voltage level varied from 100 mV to 400 mV at the frequency of 1 kHz. Figure 29(a) demonstrates that, the capacitive response decreased monotonically as the voltage increased from 100 mV to 400 mV, showing that higher AC voltage contributed to larger sensor response. When the voltage level is above 300 mV, the increase in sensor response became limited, due to saturation of binding sites on the sensor. Therefore, the optimal voltage level is determined to be 300 mV. The control samples of ultrapure water exhibited a noise limited response ranged from -0.52 to 1.26 %/min.

Figure 29(b) illustrates the frequency dependence of the sensor under a 300 mV AC signal whose frequency varied from 500 Hz to 10 kHz, with a well-defined maximum response at 1 kHz. This is in agreement with the bell-shaped frequency dependence of ACEO velocity, validating that ACEO effect is indeed the responsible mechanism for rapid and sensitive detection. Therefore, AC signal of 300 mV at 1 kHz is used in all the subsequent experiments.

7.5 Dose response

0.1 fM to 1 pM BPA samples are tested on the sensor to obtain the sensor's BPA dose response with an assay time of 20 seconds, and the results are shown in Figure 30 (a).

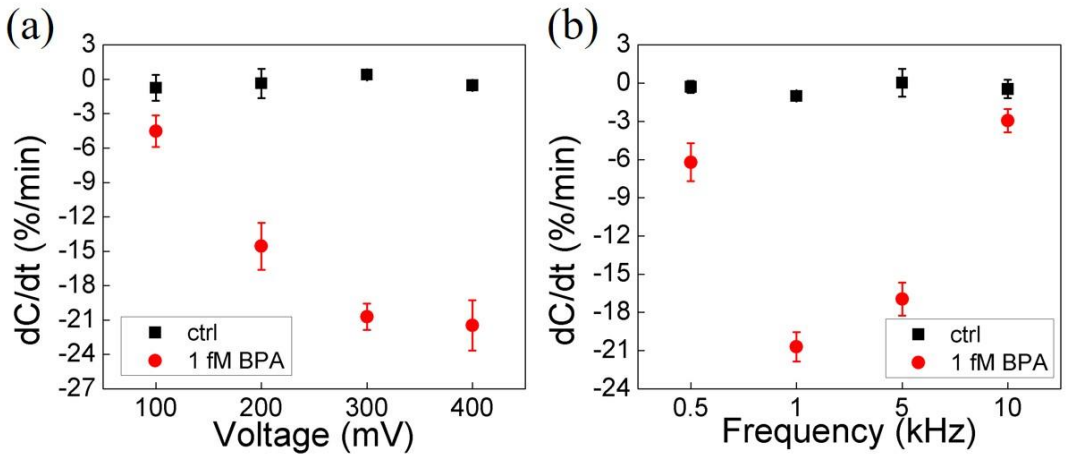

Figure 29 Response of control and 1 fM BPA samples (a) when using 1 kHz AC signal with its voltage varied from 100 mV to 400 mV and (b) when using 300 mV AC signal with its frequency varied from 500 Hz to 10 kHz.

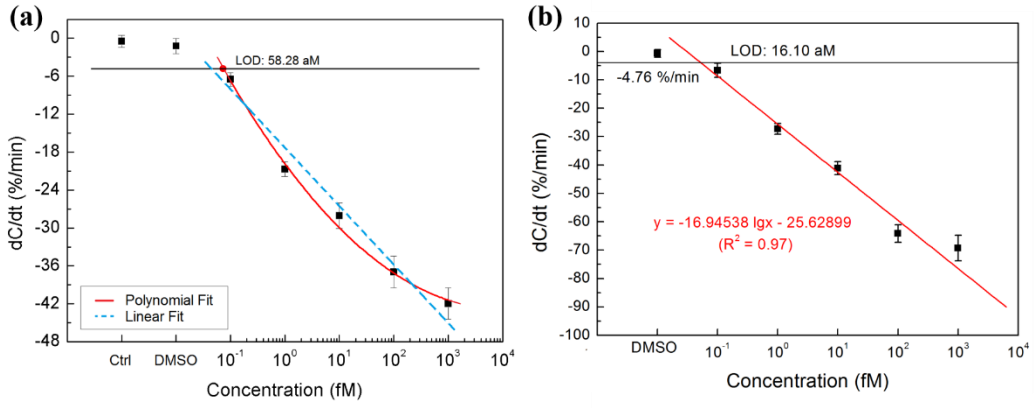

Figure 30 Detected dose response of BPA samples as a function of concentration by data obtained in (a) 20 seconds and (b) 10 seconds.

Each BPA concentration is tested in triplicate using a new sensor each time. The responses from the water samples again are shown to be negligible, -0.47±0.94 %/min. The response from DMSO which is used as solvent in initial stock solution preparations for all the test compounds is also tested. The final concentration of DMSO in working solutions of all test compounds is 1.0 ppm with a negligible response of *dC/dt* of -1.22±1.19 %/min. The magnitude of *dC/dt*, or |*dC/dt*|, increases monotonically with increasing BPA concentration from 0.1fM to 1pM, with -6.48±1.08 %/min for 100 aM BPA and -41.9±2.47 %/min for 1pM BPA. The increase in |*dC/dt*| with BPA level is slower than logarithm dependence, again due to rapid saturation of binding sites at higher BPA concentrations. Therefore, the dependence of *dC/dt* on BPA concentration is approximated by both quadratic curve and linear fittings as follow:

$$y = 1.468\lg^2 x - 11.591\lg x - 19.836 \tag{7.1}$$

$$y = -9.392\lg x - 17.885 \tag{7.2}$$

where *x* is the BPA concentration in fM and *y* is the capacitance change per minute, *dC/dt*. The correlation coefficient R^2 is 0.989 and 0.943 for the quadratic curve and linear fitting respectively. Figure 30(b) demonstrates the sensor's dose response based on the first 10 seconds' data points of the acquired sensor readout values. By analyzing the data of the first 10 seconds, binding sites' saturation effects can be diminished, allowing the sensor to each a much lower LOD of 16.10 aM. Since the quadratic fitting gives a more precise description of the characteristic of the dose response, it is adopted in the subsequent analysis.

The limit of detection is found based on the fitting curve, which is defined as 3 standard deviations (1.19 %/min) from the response of background control: DMSO (-1.22±1.19 %/min). The cut-off *dC/dt* is found to be -4.78 %/min, which corresponds to a BPA concentration of 58.28 aM.

7.6 Specificity

BPA's analogues BPS and BPF (bisphenol S and bisphenol F), and two of BPA metabolites, β-D-glucuronide and monosulfate salt, are used as interference or non-specific molecules to determine the specificity of the functionalized aptamer sensor. Their responses are shown in Figure 31. Tests are conducted with an AC signal of 300 mV and 1 kHz applied to the sensor. BPA−G and BPA-M in Figure 31 represent BPA β-D-glucuronide and monosulfate salt respectively. BPS and BPF samples are tested at 1 pM and 10 pM, and β-D-glucuronide and monosulfate salt are 100 fM and 10 pM. In Figure 31, the control samples of ultrapure water (0.44±0.64 %/min) and dimethlsulfoxide, DMSO, (-1.22±1.19 %/min), and 1 fM and 10 fM BPA results are listed as well for comparison. BPS (4.22±0.66 %/min for 1 pM and 3.29±0.09 %/min for 10 pM), BPF (5.41±1.13 %/min for 1pM and 4.25±0.26 %/min for 10 pM), and monosulfate salt (7.91±5.44 %/min for 100 fM and 0.22±1.15 %/min for 10 pM) all yielded small negative responses. However, glucuronide salt (-11.90±2.36 %/min for 100 fM and -22.33±3.20 %/min for 10 pM) yielded a positive response but only at much high level of concentrations. The 100 fM glucuronide salt's response is calculated to be equivalent to BPA's response at 0.23 fM, demonstrating that the sensor's selectivity against glucuronide is 430:1. It is known the glucuronidation and sulfation of environmental phenols are the

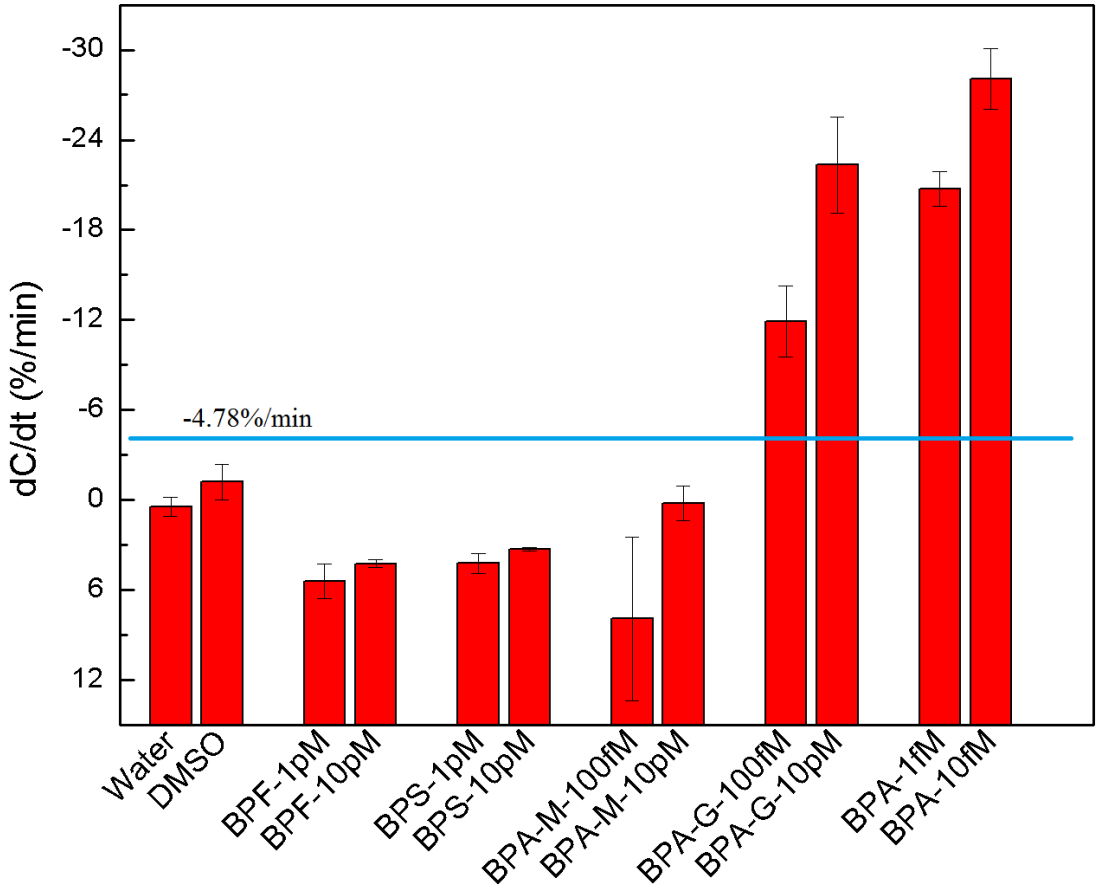

Figure 31 Illustration of sensor specificity. The blue line is the sensor response of LOD (58.28 aM)

major BPA metabolic pathways identified in human and animals.[81] Our results indicate that proper dilutions would be necessary when the same aptamer is used for free BPA detection from biological matrices.

7.7 Complex river samples

In order to test the performance of the sensor in complex matrix, and to illustrate the selectivity against various non-specific compounds, two river water samples are collected near a local waste treatment plant and diluted 1:1,000,000 in ultrapure water prior to testing. The diluted river water samples are then spiked with 5 fM BPA and performed recovery tests. The percentage recovery (% Recovery) is calculated as:

$$\%\ \text{Recovery} = \frac{C_{spiked\ river\ sample} - C_{unspiked\ river\ sample}}{5\ fM} \times 100\% \qquad (7.3)$$

BPA concentration in the river water samples are found by using Equation 6.1, i.e. solving for *x* using the measured *dC/dt* as *y*. Table 3 shows the sensor response for river water samples with the corresponding concentration interpreted using Equation 6.1. Diluted surface water sampled from up and down streams yielded a measured concentration of 0.53 fM and 0.30 fM BPA, which corresponds to original BPA concentrations of 0.53 nM and 0.30 nM respectively. Those values are in agreement with BPA levels reported in the literature.[82],[83]. The subsequent recovery experiments obtained recovery rates of 83.61% and 100.70% for 5 fM BPA added to river water.

Based on our study, the sensing mechanism can be summarized in Figure 32. Enhanced by ACEO effect, BPA particles are carried to the electrode's surface by fluid flows during capacitance measurement, together with interference particles such as BPS. Since the aptamer deposited on the electrode's surface can only bind with BPA specifically,

Table 3 Surface water samples detection and recoveries.

Sample	dC/dt [%/min]	Interpreted Concentration [fM]	Recovery [%]
Downstream	-16.48±0.63	0.53	
Mixed with 5 fM sample	-26.97±1.59	4.71	83.61
Upstream	-13.49±1.25	0.31	
Mixed with 5 fM sample	-27.49±1.83	5.34	100.70

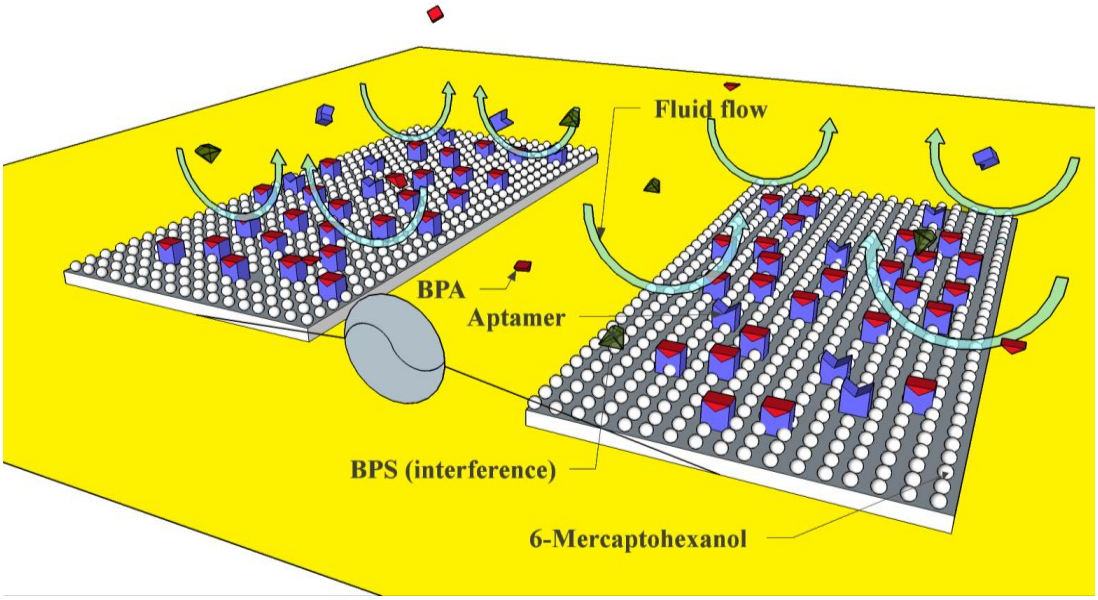

Figure 32 Ultrasensitive capacitive sensors with directed movement of complex sample particles with applied the ACEO effect.

trace concentrations of BPA increase the layer thickness and decrease the interfacial capacitance. The nanostructured surface increases the area to immobilize aptamer, significantly increasing the sensitivity.

CHAPTER 8

CONCLUSONS AND FUTURE WORK

8.1 Conclusions

This work demonstrates a low cost bio sensing platform that can be used for pathogens and infections diagnosis. By inducing ACEK for particles manipulation and acceleration, the sensing platform realizes sample enrichment and binding reaction measurement simultaneously, which leads to the sensor to be rapid, sensitive and specific. The achievements of this work include:

(1) Different electrodes are investigated to study their suitability for direct capacitive sensing method in order to support rapid and low cost biosensing. Well-designed electrodes should have lower internal resistance and an interfacial-bulk capacitance ratio that is great than at least 10^3.

(2) Much higher sensitivity in detection has been achieved using cross linkers, as well as by optimizing testing and incubation buffers. The improvement in sensor response from adopting linkers is significant in detecting influenza A virus and protein IgG . Tests of influenza A virus and protein IgG obtain LODs of 15 pg/mL and 4.513 fg/mL respectively in 30 seconds. However, without linker modification on sensor electrodes, the sensor shows quite small responses with an LOD of 1 ng/mL in protein IgG detection and is not even able to differentiate various concentrations of influenza A virus analytical samples. In addition to linkers, various incubation and testing buffers are also critical to bioparticles detection. After optimization of incubation and testing

buffers in nuclei acid detection, specific detection of human herpesvirus-1 (HSV-1) dsDNA can be achieved within 30 seconds with an LOD of 1 pg/mL (6.5 copies/μL or 10.7 aM) in standard buffer, and 20 pg/mL (129.5 copies/μL or 0.21 fM) in neat serum.

(3) This bio-sensing platform can be expanded to chemical detection. Chemicals are very small molecules compared with virus or proteins, and DEP is not able to contribute in this application. AC electroosmotic effect, however, can be utilized for enrichment of small molecules, expanding the varieties of ACEK capacitive sensing, as well as the application in chemical detection. Detection of bisphenol A (BPA) by electrodes on flexible polyimide substrate possesses selectivity and an LOD of 58.28 aM corresponding to a rapid integration time of only 20 seconds. As for the complex samples, the sensor reaches 83.61% and 100.70% recovery of two surface water samples.

To summarize, this work demonstrates a successful development of innovative sensors for virus, protein, nuclei acid and small chemical molecules detection at ultra low concentration. This research provides a framework of low cost and practical sensing for on-site disease diagnosis and environmental monitoring.

8.2 Future work

Firstly, this developed bio-sensing platform is very promising for detecting target particles in complex matrix. Currently, the sensor is demonstrated to work with diluted serum samples. In the future, we will try to integrate the sensor with a wicking material, such as a piece of filter paper, on top of the sensing area for sample load. By doing so, it is

anticipated that the wicking material will retain the blood cells and allow smaller particles such as proteins to move towards the sensor by capillary force, thus making it possible for the sensor to work with whole blood directly.

Secondly, with integration of a board-level capacitance measuring and readout system, this platform can be realized into a portable device with multiple channels used for on-site sensing, monitoring and screening tests.

LIST OF REFERENCES

[1] L. C. Clark, “Monitor and control of blood and tissue oxygenation,” *Trans Am. Soc. Artif. Intern. Organs*, vol. 2, pp. 41–48, 1956.
[2] W. R. Heineman and W. B. Jensen, “Leland C. Clark Jr. (1918–2005),” *Biosens. Bioelectron.*, vol. 21, no. 8, pp. 1403–1404, Feb. 2006.
[3] A. P. F. Turner, “Biosensors: sense and sensibility,” *Chem. Soc. Rev.*, vol. 42, no. 8, p. 3184, 2013.
[4] V. Sikka *et al.*, “The emergence of zika virus as a global health security threat: A review and a consensus statement of the INDUSEM Joint working Group (JWG),” *J. Glob. Infect. Dis.*, vol. 8, no. 1, p. 3, 2016.
[5] I. I. Bogoch *et al.*, “Anticipating the international spread of Zika virus from Brazil,” *The Lancet*, vol. 387, no. 10016, pp. 335–336, Jan. 2016.
[6] M. R. Duffy *et al.*, “Zika Virus Outbreak on Yap Island, Federated States of Micronesia,” *N. Engl. J. Med.*, vol. 360, no. 24, pp. 2536–2543, Jun. 2009.
[7] WHO, “Zika virus and complications: Questions and answers,” 28-Jul-2016. [Online]. Available: http://www.who.int/features/qa/zika/en/.
[8] S. JAMES, “Global Bisphenol A (BPA) Market By Application (Appliances, Automotive, Consumer, Construction, Electrical & Electronics) Expected To Reach USD 20.03 Billion by 2020,” Jun-2014.
[9] E. R. Hugo, T. D. Brandebourg, J. G. Woo, J. Loftus, J. W. Alexander, and N. Ben-Jonathan, “Bisphenol A at Environmentally Relevant Doses Inhibits Adiponectin Release from Human Adipose Tissue Explants and Adipocytes,” *Environ. Health Perspect.*, vol. 116, no. 12, pp. 1642–1647, Aug. 2008.
[10] R. R. Newbold, W. N. Jefferson, and E. Padilla-Banks, “Prenatal Exposure to Bisphenol A at Environmentally Relevant Doses Adversely Affects the Murine Female Reproductive Tract Later in Life,” *Environ. Health Perspect.*, vol. 117, no. 6, pp. 879–885, Jun. 2009.
[11] H. Cui, J. Wu, S. Eda, J. Chen, W. Chen, and L. Zheng, “Rapid capacitive detection of femtomolar levels of bisphenol A using an aptamer-modified disposable microelectrode array,” *Microchim. Acta*, vol. 182, no. 13–14, pp. 2361–2367, Oct. 2015.
[12] R. Fogel and J. Limson, “Developing Biosensors in Developing Countries: South Africa as a Case Study,” *Biosensors*, vol. 6, no. 1, p. 5, Feb. 2016.
[13] A. P. F. Turner, I. Karube, and G. S. Wilson, Eds., *Biosensors: fundamentals and applications*. Oxford [Oxfordshire] ; New York: Oxford University Press, 1987.
[14] N. J. Ronkainen, H. B. Halsall, and W. R. Heineman, “Electrochemical biosensors,” *Chem. Soc. Rev.*, vol. 39, no. 5, p. 1747, 2010.
[15] Y. Wan, Y. Su, X. Zhu, G. Liu, and C. Fan, “Development of electrochemical immunosensors towards point of care diagnostics,” *Biosens. Bioelectron.*, vol. 47, pp. 1–11, Sep. 2013.
[16] D. R. Thévenot, K. Toth, R. A. Durst, and G. S. Wilson, “Electrochemical biosensors: recommended definitions and classification1International Union of Pure and Applied Chemistry: Physical Chemistry Division, Commission I.7 (Biophysical Chemistry); Analytical Chemistry Division, Commission V.5 (Electroanalytical Chemistry).1,” *Biosens. Bioelectron.*, vol. 16, no. 1–2, pp. 121–131, Jan. 2001.

[17] M. ’delanji Vestergaard, K. Kerman, and E. Tamiya, “An Overview of Label-free Electrochemical Protein Sensors,” *Sensors*, vol. 7, no. 12, pp. 3442–3458, Dec. 2007.
[18] Y. Wang, H. Xu, J. Zhang, and G. Li, “Electrochemical Sensors for Clinic Analysis,” *Sensors*, vol. 8, no. 4, pp. 2043–2081, Mar. 2008.
[19] M. Morikawa, N. Kimizuka, M. Yoshihara, and T. Endo, “New Colorimetric Detection of Glucose by Means of Electron-Accepting Indicators: Ligand Substitution of [Fe(acac)3−n(phen)n]n+ Complexes Triggered by Electron Transfer from Glucose Oxidase,” *Chem. - Eur. J.*, vol. 8, no. 24, pp. 5580–5584, Dec. 2002.
[20] Y. Miwa, M. Nishizawa, T. Matsue, and I. Uchida, “A Conductometric Glucose Sensor Based on a Twin-Microband Electrode Coated with a Polyaniline Thin Film.,” *Bull. Chem. Soc. Jpn.*, vol. 67, no. 10, pp. 2864–2866, 1994.
[21] S. Mansouri and J. S. Schultz, “A Miniature Optical Glucose Sensor Based on Affinity Binding,” *Bio/Technology*, vol. 2, no. 10, pp. 885–890, Oct. 1984.
[22] J. C. Pickup, F. Hussain, N. D. Evans, O. J. Rolinski, and D. J. S. Birch, “Fluorescence-based glucose sensors,” *Biosens. Bioelectron.*, vol. 20, no. 12, pp. 2555–2565, Jun. 2005.
[23] E.-H. Yoo and S.-Y. Lee, “Glucose Biosensors: An Overview of Use in Clinical Practice,” *Sensors*, vol. 10, no. 5, pp. 4558–4576, May 2010.
[24] C. A. Rowe-Taitt, J. W. Hazzard, K. E. Hoffman, J. J. Cras, J. P. Golden, and F. S. Ligler, “Simultaneous detection of six biohazardous agents using a planar waveguide array biosensor,” *Biosens. Bioelectron.*, vol. 15, no. 11–12, pp. 579–589, Dec. 2000.
[25] X. Liu, K. Yang, A. Wadhwa, S. Eda, S. Li, and J. Wu, “Development of an AC electrokinetics-based immunoassay system for on-site serodiagnosis of infectious diseases,” *Sens. Actuators Phys.*, vol. 171, no. 2, pp. 406–413, Nov. 2011.
[26] S. Haeberle and R. Zengerle, “Microfluidic platforms for lab-on-a-chip applications,” *Lab. Chip*, vol. 7, no. 9, p. 1094, 2007.
[27] R. M. Lequin, “Enzyme Immunoassay (EIA)/Enzyme-Linked Immunosorbent Assay (ELISA),” *Clin. Chem.*, vol. 51, no. 12, pp. 2415–2418, Dec. 2005.
[28] X. Yang, J. Janatova, J. M. Juenke, G. A. McMillin, and J. D. Andrade, “An ImmunoChip prototype for simultaneous detection of antiepileptic drugs using an enhanced one-step homogeneous immunoassay,” *Anal. Biochem.*, vol. 365, no. 2, pp. 222–229, Jun. 2007.
[29] G. Blagoi, S. Keller, A. Johansson, A. Boisen, and M. Dufva, “Functionalization of SU-8 photoresist surfaces with IgG proteins,” *Appl. Surf. Sci.*, vol. 255, no. 5, pp. 2896–2902, Dec. 2008.
[30] Y. Gao, F. Y. H. Lin, G. Hu, P. M. Sherman, and D. Li, “Development of a novel electrokinetically driven microfluidic immunoassay for the detection of Helicobacter pylori,” *Anal. Chim. Acta*, vol. 543, no. 1–2, pp. 109–116, Jul. 2005.
[31] D. Hoegger, P. Morier, C. Vollet, D. Heini, F. Reymond, and J. S. Rossier, “Disposable microfluidic ELISA for the rapid determination of folic acid content in food products,” *Anal. Bioanal. Chem.*, vol. 387, no. 1, pp. 267–275, Dec. 2006.
[32] F. Y. H. Lin, M. Sabri, D. Erickson, J. Alirezaie, D. Li, and P. M. Sherman, “Development of a novel microfluidic immunoassay for the detection of Helicobacter pylori infection,” *The Analyst*, vol. 129, no. 9, p. 823, 2004.

[33] L. Yu, Y. Liu, Y. Gan, and C. M. Li, "High-performance UV-curable epoxy resin-based microarray and microfluidic immunoassay devices," *Biosens. Bioelectron.*, vol. 24, no. 10, pp. 2997–3002, Jun. 2009.
[34] X. Zhao and S. A. Shippy, "Competitive Immunoassay for Microliter Protein Samples with Magnetic Beads and Near-Infrared Fluorescence Detection," *Anal. Chem.*, vol. 76, no. 7, pp. 1871–1876, Apr. 2004.
[35] K. Sato *et al.*, "Integration of an Immunosorbent Assay System: Analysis of Secretory Human Immunoglobulin A on Polystyrene Beads in a Microchip," *Anal. Chem.*, vol. 72, no. 6, pp. 1144–1147, Mar. 2000.
[36] A. W. Martinez, S. T. Phillips, M. J. Butte, and G. M. Whitesides, "Patterned Paper as a Platform for Inexpensive, Low-Volume, Portable Bioassays," *Angew. Chem. Int. Ed.*, vol. 46, no. 8, pp. 1318–1320, Feb. 2007.
[37] E. Fu, B. Lutz, P. Kauffman, and P. Yager, "Controlled reagent transport in disposable 2D paper networks," *Lab. Chip*, vol. 10, no. 7, p. 918, 2010.
[38] A. W. Martinez, S. T. Phillips, G. M. Whitesides, and E. Carrilho, "Diagnostics for the Developing World: Microfluidic Paper-Based Analytical Devices," *Anal. Chem.*, vol. 82, no. 1, pp. 3–10, Jan. 2010.
[39] B. B. Haab, "Methods and applications of antibody microarrays in cancer research," *PROTEOMICS*, vol. 3, no. 11, pp. 2116–2122, Nov. 2003.
[40] H. Jiang, X. Weng, and D. Li, "Microfluidic whole-blood immunoassays," *Microfluid. Nanofluidics*, vol. 10, no. 5, pp. 941–964, May 2011.
[41] J. Homola, S. S. Yee, and G. Gauglitz, "Surface plasmon resonance sensors: review," *Sens. Actuators B Chem.*, vol. 54, no. 1–2, pp. 3–15, Jan. 1999.
[42] H. Tanaka, M. Hanasaki, T. Isojima, H. Takeuchi, T. Shiroya, and H. Kawaguchi, "Enhancement of sensitivity of SPR protein microarray using a novel 3D protein immobilization," *Colloids Surf. B Biointerfaces*, vol. 70, no. 2, pp. 259–265, May 2009.
[43] M. H. F. Meyer, M. Hartmann, and M. Keusgen, "SPR-based immunosensor for the CRP detection—A new method to detect a well known protein," *Biosens. Bioelectron.*, vol. 21, no. 10, pp. 1987–1990, Apr. 2006.
[44] T. Endo, K. Kerman, N. Nagatani, Y. Takamura, and E. Tamiya, "Label-Free Detection of Peptide Nucleic Acid−DNA Hybridization Using Localized Surface Plasmon Resonance Based Optical Biosensor," *Anal. Chem.*, vol. 77, no. 21, pp. 6976–6984, Nov. 2005.
[45] S. Sabban, "Development of an in vitro model system for studying the interaction of Equus caballus IgE with its high- affinity FcεRI receptor," PhD Thesis, The University of Sheffield, 2011.
[46] F.-C. Chien and S.-J. Chen, "A sensitivity comparison of optical biosensors based on four different surface plasmon resonance modes," *Biosens. Bioelectron.*, vol. 20, no. 3, pp. 633–642, Oct. 2004.
[47] B. Liedberg, C. Nylander, and I. Lunström, "Surface plasmon resonance for gas detection and biosensing," *Sens. Actuators*, vol. 4, pp. 299–304, Jan. 1983.

[48] R. P. H. Kooyman, H. Kolkman, J. Van Gent, and J. Greve, “Surface plasmon resonance immunosensors: sensitivity considerations,” *Anal. Chim. Acta*, vol. 213, pp. 35–45, 1988.
[49] V. Owen, “Real-time optical immunosensors — A commercial reality,” *Biosens. Bioelectron.*, vol. 12, no. 1, pp. i–ii, Jan. 1997.
[50] K. A. Peterlinz, R. M. Georgiadis, T. M. Herne, and M. J. Tarlov, “Observation of Hybridization and Dehybridization of Thiol-Tethered DNA Using Two-Color Surface Plasmon Resonance Spectroscopy,” *J. Am. Chem. Soc.*, vol. 119, no. 14, pp. 3401–3402, Apr. 1997.
[51] L. S. Jung, C. T. Campbell, T. M. Chinowsky, M. N. Mar, and S. S. Yee, “Quantitative Interpretation of the Response of Surface Plasmon Resonance Sensors to Adsorbed Films,” *Langmuir*, vol. 14, no. 19, pp. 5636–5648, Sep. 1998.
[52] J. Homola, S. S. Yee, and G. Gauglitz, “Surface plasmon resonance sensors: review,” *Sens. Actuators B Chem.*, vol. 54, no. 1–2, pp. 3–15, Jan. 1999.
[53] M. C. Rodriguez, A.-N. Kawde, and J. Wang, “Aptamer biosensor for label-free impedance spectroscopy detection of proteins based on recognition-induced switching of the surface charge,” *Chem. Commun.*, no. 34, p. 4267, 2005.
[54] E. Katz and I. Willner, “Probing Biomolecular Interactions at Conductive and Semiconductive Surfaces by Impedance Spectroscopy: Routes to Impedimetric Immunosensors, DNA-Sensors, and Enzyme Biosensors,” *Electroanalysis*, vol. 15, no. 11, pp. 913–947, Jul. 2003.
[55] J.-G. Guan, Y.-Q. Miao, and Q.-J. Zhang, “Impedimetric biosensors,” *J. Biosci. Bioeng.*, vol. 97, no. 4, pp. 219–226, Jan. 2004.
[56] I. O. K’Owino and O. A. Sadik, “Impedance Spectroscopy: A Powerful Tool for Rapid Biomolecular Screening and Cell Culture Monitoring,” *Electroanalysis*, vol. 17, no. 23, pp. 2101–2113, Dec. 2005.
[57] M. I. Prodromidis, “Impedimetric immunosensors—A review,” *Electrochimica Acta*, vol. 55, no. 14, pp. 4227–4233, May 2010.
[58] P. Bataillard, F. Gardies, N. Jaffrezic-Renault, C. Martelet, B. Colin, and B. Mandrand, “Direct detection of immunospecies by capacitance measurements,” *Anal. Chem.*, vol. 60, no. 21, pp. 2374–2379, Nov. 1988.
[59] J. Wu, “Interactions of electrical fields with fluids:laboratory-on-a-chip applications,” *IET Nanobiotechnol.*, vol. 2, no. 1, pp. 14–27, 2008.
[60] K. Yang and J. Wu, “Numerical study of in situ preconcentration for rapid and sensitive nanoparticle detection,” *Biomicrofluidics*, vol. 4, no. 3, p. 034106, 2010.
[61] J. Wu, Y. Ben, and H.-C. Chang, “Particle detection by electrical impedance spectroscopy with asymmetric-polarization AC electroosmotic trapping,” *Microfluid. Nanofluidics*, vol. 1, no. 2, pp. 161–167, May 2005.
[62] J. Wu, “Advances of LOC-Based Particle Manipulation by AC Electrical Fields,” *Recent Pat. Electr. Eng.*, vol. 1, no. 3, pp. 178–187, Nov. 2008.
[63] A. Castellanos, A. Ramos, A. González, N. G. Green, and H. Morgan, “Electrohydrodynamics and dielectrophoresis in microsystems: scaling laws,” *J. Phys. Appl. Phys.*, vol. 36, pp. 2584–2597, 2003.

[64] N. G. Green, A. Ramos, A. González, H. Morgan, and A. Castellanos, "Fluid flow induced by nonuniform ac electric fields in electrolytes on microelectrodes. I. Experimental measurements," *Phys. Rev. E*, vol. 61, no. 4, pp. 4011–4018, Apr. 2000.
[65] N. Islam, M. Lian, and J. Wu, "Enhancing microcantilever capability with integrated AC electroosmotic trapping," *Microfluid. Nanofluidics*, vol. 3, no. 3, pp. 369–375, Apr. 2007.
[66] J. Wu and N. Islam, "A Simple Method to Integrate In Situ Nano-Particle Focusing With Cantilever Detection," *IEEE Sens. J.*, vol. 7, no. 6, pp. 957–958, Jun. 2007.
[67] J. Wu, Y. Ben, D. Battigelli, and H.-C. Chang, "Long-Range AC Electroosmotic Trapping and Detection of Bioparticles," *Ind. Eng. Chem. Res.*, vol. 44, no. 8, pp. 2815–2822, Apr. 2005.
[68] A. Ramos, H. Morgan, N. Green, and A. Castellanos, "AC electrokinetics: a review of forces in microelectrode structures," *J. Phys. Appl. Phys.*, vol. 31, no. 18, pp. 2338–2353, 1998.
[69] S. Li *et al.*, "AC electrokinetics-enhanced capacitive immunosensor for point-of-care serodiagnosis of infectious diseases," *Biosens. Bioelectron.*, vol. 51, pp. 437–443, Jan. 2014.
[70] B. T. Least and D. A. Willis, "Modification of polyimide wetting properties by laser ablated conical microstructures," *Appl. Surf. Sci.*, vol. 273, pp. 1–11, May 2013.
[71] H. Cui, C. Cheng, J. Wu, and S. Eda, "Rapid detection of progesterone by commercially available microelectrode chips," 2013, pp. 1–4.
[72] S. Li *et al.*, "Alternating current electrokinetics enhanced in situ capacitive immunoassay: Microfluidics and Miniaturization," *ELECTROPHORESIS*, vol. 36, no. 3, pp. 471–474, Feb. 2015.
[73] H. Cui *et al.*, "An AC electrokinetic impedance immunosensor for rapid detection of tuberculosis," *The Analyst*, vol. 138, no. 23, pp. 7188–7196, 2013.
[74] W. Zhongliang *et al.*, "Detection of the four major human herpesviruses simultaneously in whole blood and cerebrospinal fluid samples by the fluorescence polarization assay," *Int. J. Infect. Dis.*, vol. 14, no. 10, pp. e893–e897, Oct. 2010.
[75] C. Cheng *et al.*, "An unamplified RNA sensor for on-site screening of Zika virus disease in a limited resource setting," *ChemElectroChem*, Jan. 2017.
[76] "M4RT," *Thermo Fisher Scientific*. [Online]. Available: http://www.remel.com/Catalog/Item.aspx?name=M4RT%-3csup%-3e%-26reg%-3b%-3c%-2fsup%-3e.
[77] K. Pardee *et al.*, "Rapid, Low-Cost Detection of Zika Virus Using Programmable Biomolecular Components," *Cell*, vol. 165, no. 5, pp. 1255–1266, May 2016.
[78] R.-Z. Li *et al.*, "High-rate in-plane micro-supercapacitors scribed onto photo paper using in situ femtolaser-reduced graphene oxide/Au nanoparticle microelectrodes," *Energy Env. Sci*, vol. 9, pp. 1458–1467, 2016.
[79] C. Zheng *et al.*, "Femtosecond Laser Fabrication of Cavity Microball Lens (CMBL) inside a PMMA Substrate for Super-Wide Angle Imaging," *Small*, vol. 11, no. 25, pp. 3007–3016, Jul. 2015.

[80] R. Rahimi, M. Ochoa, W. Yu, and B. Ziaie, “Highly Stretchable and Sensitive Unidirectional Strain Sensor via Laser Carbonization,” *ACS Appl. Mater. Interfaces*, vol. 7, no. 8, pp. 4463–4470, Mar. 2015.

[81] N. Shangari, T. S. Chan, and P. J. O’Brien, “Sulfation and Glucuronidation of Phenols: Implications in Coenyzme Q Metabolism,” in *Methods in Enzymology*, vol. 400, Elsevier, 2005, pp. 342–359.

[82] V. A. Santhi, N. Sakai, E. D. Ahmad, and A. M. Mustafa, “Occurrence of bisphenol A in surface water, drinking water and plasma from Malaysia with exposure assessment from consumption of drinking water,” *Sci. Total Environ.*, vol. 427–428, pp. 332–338, Jun. 2012.

[83] G. M. Klečka, C. A. Staples, K. E. Clark, N. van der Hoeven, D. E. Thomas, and S. G. Hentges, “Exposure Analysis of Bisphenol A in Surface Water Systems in North America and Europe,” *Environ. Sci. Technol.*, vol. 43, no. 16, pp. 6145–6150, Aug. 2009.

VITA

Cheng Cheng joined The University of Tennessee at Knoxville in August 2012 to pursue the Ph.D. degree in Electrical Engineering. He received his Master of Science from Morehead State University in May 2012 and his Bachelor of Engineering from Guangxi University, China in 2010. His research focus includes biomedical sensing instrumentation and device application.